Applied Mathematical Modelling 162 (2027) 117225

Contents lists available at ScienceDirect

Applied Mathematical Modelling

journal homepage: www.elsevier.com/locate/apm

Pathogen evolution under strategy changes in vaccination campaigns: A game-theoretic framework

Qiutong Liu [a], Stacey R. Smith? [b,*], Yanni Xiao [a,*]

[a] School of Mathematics and Statistics, Xi'an Jiaotong University, Xi'an, 710049, PR China
[b] Department of Mathematics and Faculty of Medicine, The University of Ottawa, Ottawa, ON, K1N 6N5, Canada

ARTICLE INFO

Keywords:
Pathogen evolution
Vaccination
Game-theoretic framework
Adaptation rates

ABSTRACT

In existing models of pathogen evolution under voluntary vaccination, vaccination behaviour is typically assumed to be static, overlooking the conflicts between individual and collective interests. To address this, we develop a multi-scale model within a game-theoretic framework that couples the dynamic processes of disease transmission, vaccination decision-making, and pathogen evolution. By reformulating vaccine uptake as a time-dependent strategic choice and incorporating a heterogeneous update mechanism, we establish the evolutionary model of vaccination strategies. Numerical results show that heterogeneous updating rules will capture autonomous population decision-making. The co-evolutionary dynamics are highly sensitive to the evolutionary adaptation rates and exhibit an asymmetric relationship between population and evolutionary dynamics. At the early stage of a vaccination scenario, we observe that imitation behaviour dominates due to limited information. Enhancing vaccine uptake is effective in limiting the emergence of detrimental variants, and the long-term evolutionary outcome may favour the emergence of specialist variants. This framework provides quantitative methods and key methodological advancements for multi-scale mathematical modelling in the context of pathogen evolution.

1. Introduction

Infectious diseases have long posed a threat to public health, raising concerns among both the public and health authorities. Vaccination has significantly benefited public health and is regarded as one of the most effective strategies for controlling infectious diseases, despite the imperfect immunity provided by most vaccines and the implementation of voluntary vaccination policies [1,2]. Evidence suggests that, under a voluntary vaccination policy, the perception of benefiting from others' contributions may erode herd immunity, thus worsening the situation [3,4]. This reflects the behavioural paradox between group interest and self-interest. Therefore, it is crucial to couple the epidemiological process with the vaccination decision-making process to consider this vaccination dilemma.

Many pathogens exhibit extensive genetic variation and can therefore readily adapt to external environments [5]. The ongoing evolution significantly influences the transmission dynamics by shaping heterogeneities in virulence, transmissibility, etc. [6–8]. Pathogen adaptation occurs when a novel variant demonstrates greater fitness in the current environment compared to its predecessor [9]. Host immunity induced by vaccination leads to a profound alteration of the current environment for pathogens [9,10]. The large epidemiological perturbations induced by vaccination also substantially alter the natural selective pressures acting on pathogen populations [5,10]. Given the scale of the global vaccination campaign against COVID-19 and the rapid emergence of new variants,

* Corresponding authors.
E-mail addresses: lqt19971018@stu.xjtu.edu.cn (Q. Liu), stacey.smith@uottawa.ca (S.R. Smith?), yxiao@mail.xjtu.edu.cn (Y. Xiao).

https://doi.org/10.1016/j.apm.2026.117225
Received 3 March 2026; Received in revised form 17 July 2026; Accepted 28 July 2026
Available online 29 July 2026

attention has increasingly shifted toward the potential impact of vaccination on viral evolution [9]. Nevertheless, few studies have explored how pathogens evolve in response to vaccination, which is the focus of this work.

Over the past few decades, there has been a substantial increase in the use of mathematical models to study pathogen evolutionary processes [9–14]. Most existing studies rely on the assumption that evolutionary dynamics unfold on a timescale that is substantially slower than that of epidemiological processes [12,14–16]. However, this assumption is unlikely to hold for many pathogens. The application of Price's equation in evolutionary epidemiology has provided an alternative framework for conceptualizing the evolution of infectious diseases, as it clearly disentangles the direct effects of natural selection from those arising through epidemiological feedbacks, while allowing these feedbacks to operate on timescales comparable to evolutionary change [10,17–19]. To avoid the assumption of mismatched timescales between evolutionary and epidemiological dynamics, Day & Gandon [18] proposed an evolutionary trait model based on Price's equation, which is tied to general evolutionary principles and closely connected to the population-genetic literature [17,19]. However, studies of pathogen evolutionary processes in the context of vaccination remain relatively limited. Moreover, most of these studies assume static vaccination strategies [9,10,14], in which the vaccine uptake in the population is treated as a constant. Nevertheless, vaccination is a behavioural strategy that may be influenced by the actions of others and by the current disease spread, which is therefore a time-dependent variable.

Evolutionary game theory has been successfully applied in recent years to model the vaccination dilemma [20–24]. Within this framework, voluntary vaccination is treated as a time-dependent strategic choice, whereby individuals make vaccination decisions by weighing the associated costs and benefits. Imitation dynamics are among the most commonly used approaches for describing strategic changes in vaccination games [3,25–27]. This mechanism assumes that individuals adjust their strategies by imitating peers who are more successful. However, in reality, an individual's strategy depends not only on interactions with the surrounding environment but also on self-assessment [28]. Individuals evaluate their perceived payoffs against an aspiration level. If the perceived payoff exceeds this aspiration level, they continue with the same strategy; otherwise, they switch to an alternative [29–31]. This mechanism is known as aspiration dynamics. It is plausible to assume that vaccination strategies are shaped by both imitation and aspiration mechanisms, an area that has received limited attention thus far.

Disease transmission, vaccination behaviour, and pathogen evolution are tightly coupled and interact with one another. However, to the best of our knowledge, no detailed studies have yet characterized the joint dynamics generated by the interplay among these three processes. Existing evolutionary epidemiological models of vaccination have mainly focused on pathogen evolution under fixed vaccination coverage, whereas vaccination game models have typically treated pathogen traits as fixed and focused on the behavioural response of individuals to disease risk and vaccination costs. Thus, these two lines of research have largely developed separately.

Motivated by these gaps, this study develops a coupled multiscale modelling framework that integrates epidemic transmission, pathogen trait evolution and adaptive vaccination behaviour (see Fig. 1). In contrast to previous evolutionary epidemiological models with static vaccination strategies, vaccine uptake is treated here as a dynamic behavioural variable. In contrast to standard vaccination game models, the epidemiological environment is not fixed by pathogens with constant traits but is rather shaped by pathogen evolution. Moreover, vaccination behaviour is assumed to be governed by both imitation and aspiration mechanisms, allowing individuals to respond not only to the strategies of others but also to their own perceived payoff relative to an aspiration level. The main novelty of our work is therefore the explicit coupling of vaccination game dynamics with evolutionary epidemiological dynamics, in which vaccine uptake and pathogen traits evolve simultaneously and feed back into disease transmission. Within this framework, we consider imperfect vaccines and voluntary vaccination in order to reflect a more realistic epidemiological setting. We then investigate the long-term impact of pathogen evolution on disease transmission and the evolutionary direction of strain types during the vaccination period.

The rest of our paper is organized as follows. In Section 2, we develop a multi-scale epidemiological model within a game-theoretic framework, considering imperfect vaccines and voluntary vaccination, and obtain the threshold R_0 for disease persistence or extinction. In Section 3, based on Price's equation, we establish our evolutionary model for pathogen virulence and examine the positivity and boundedness of the trait model. Numerical simulations are performed to study the long-term impact of pathogen evolution on disease transmission. Next, we focus on immunity-adapted variants during the vaccination period, quantify the evolutionary direction of strain types and parameterize the proposed model using the empirical data in Section 4. Further, we analyze the degenerate evolutionary vaccination model, where there is no distinction between vaccinated and unvaccinated populations, and we examine its dynamical behaviour in Section 5. We conclude with a discussion.

2. Epidemiological model with dynamic vaccination strategy

2.1. Transmission process

We use a classical SIR framework that accounts for imperfect vaccination to describe the transmission process. The host population is assumed to be divided into three classes: susceptible S, infectious I and recovered R. Assume that susceptible individuals choose either a vaccination (v) or a non-vaccination (n) strategy. Let p denote the fraction of newly susceptible individuals who adopt the vaccination strategy (i.e., vaccine uptake) and the remaining fraction $1-p$ represents newly susceptible individuals who adopt the non-vaccination strategy. The fraction p is dynamic and evolves over time according to the principles of evolutionary game theory, which will be discussed in detail later. When a susceptible host is vaccinated, its internal environment changes, affecting the replication of the pathogen within the host. Therefore, there is an inherent difference between vaccinated and unvaccinated hosts; consequently, infected individuals should also be divided into two subclasses: I_n and I_v. It should be noted that, owing to the presence of natural immunity, infected hosts are not assumed to alter their strategy. The disease-transmission model is governed by

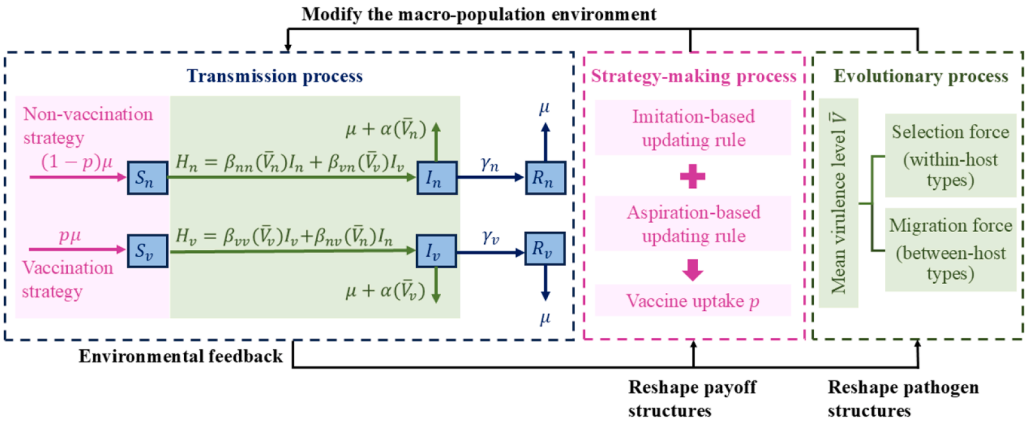

Fig. 1. Schematic diagram illustrating the coupling of the disease-transmission process, the strategy-making process and the evolutionary process.

the following ordinary differential equations:

$$\begin{aligned}
\frac{dS_n}{dt} &= (1-p)\mu - \beta_{nn}I_nS_n - \beta_{vn}I_vS_n - \mu S_n,\\
\frac{dS_v}{dt} &= p\mu - \beta_{nv}I_nS_v - \beta_{vv}I_vS_v - \mu S_v,\\
\frac{dI_n}{dt} &= S_n(\beta_{nn}I_n + \beta_{vn}I_v) - \alpha_nI_n - \gamma_nI_n - \mu I_n,\\
\frac{dI_v}{dt} &= S_v(\beta_{nv}I_n + \beta_{vv}I_v) - \alpha_vI_v - \gamma_vI_v - \mu I_v,\\
\frac{dR_n}{dt} &= \gamma_nI_n - \mu R_n,\\
\frac{dR_v}{dt} &= \gamma_vI_v - \mu R_v.
\end{aligned} \tag{1}$$

Susceptible individuals who choose vaccination (S_v) or non-vaccination (S_n) may become infected and transition to the corresponding infectious compartment, I_v or I_n, respectively. The fraction of vaccinators among the newly susceptible population is given by p. The mean transmission rate of the pathogen from a host of type j to a host of type z, where $j, z \in \{v, n\}$ indicate vaccinated or non-vaccinated individuals, is denoted by β_{jz}. Specifically, we assume $\beta_{jz} = \beta_j\theta_z$, where β_j characterizes the transmissibility of an infectious individual of type j, and θ_z denotes the susceptibility of a host of type z (with $\theta_n > \theta_v$). Parameters γ_n and γ_v denote the mean recovery rates, while α_n and α_v represent the mean disease-induced mortality rates in non-vaccinated (naïve) and vaccinated hosts, respectively. The natural birth/death rate is given by μ. All parameters are nonnegative. Here, S_n, S_v, I_n, I_v, R_n and R_v represent fractions of the population instead of absolute numbers.

2.2. The vaccination strategy-making process

In the following, we examine the evolution of the vaccine uptake p using the framework of evolutionary game theory. This explicitly involves reframing the fraction of vaccinators p as a time-dependent behavioural variable $p(t)$. Assume that the expected payoffs for vaccinators P_v and for non-vaccinators P_n are recognized as the negative of the costs and increase linearly with the current disease prevalence $I = I_n + I_v$ [32]. In addition, we suppose that individuals adopting the vaccinating strategy pay a constant additional cost k. Thus, we have

$$P_n(\tau) = -c_nI(\tau), \quad P_v(\tau) = -c_vI(\tau) - k,$$

where c_v and c_n represent the perceived risk of infection for vaccinated and unvaccinated individuals, respectively, with $c_n > c_v$.

Vaccinating decisions can be influenced by imitation as well as self-evaluation (or aspiration). Next, we analyze vaccinating behaviour by coupling both imitation and aspiration update rules based on the method in [29], which lies within the framework of a mean-field approximation in an infinitely large, well-mixed population. The master equation [29,33] that characterizes the evolution of vaccination strategies under the mean-field framework, integrating both mechanisms, is given by:

$$\frac{dp}{d\tau} = \xi p(1-p)(F_{nv} - F_{vn}) + (1-\xi)[(1-p)F_n^a - pF_v^a]. \tag{2}$$

Here, τ denotes the time unit for strategy change and ξ weighs the relative importance of the imitation mechanism compared to the aspiration mechanism on decision-making, where $\xi \in [0, 1]$. F_{nv} (resp., F_{vn}) denotes the switching probability from non-vaccinated to vaccinated (resp., from vaccinated to non-vaccinated) through the imitation process. F_n^a and F_v^a are the switching probabilities of non-vaccinators and vaccinators, respectively, under aspiration-based update rules. The term $p(1-p)(F_{nv} - F_{vn})$ depicts the imitation

protocol, whereas the term $(1-p)F_n^a - pF_v^a$ represents the aspiration protocol. In particular, $\xi = 1$ (resp., $\xi = 0$) corresponds to the pure imitation (resp., aspiration) dynamics; i.e., pure updating-rule case. Model (2) offers greater versatility by encompassing scenarios ranging from purely imitation-driven strategy-making to more general cases, thereby better reflecting real-world dynamics. The switching probabilities F_{nv}, F_{vn}, F_n^a and F_v^a depend on the payoffs P_n and P_v. We employ Fermi functions to characterize these switching probabilities as follows:

$$
\begin{aligned}
F_{nv} &= \frac{1}{1+e^{-h(P_v-P_n)}} = \frac{1}{1+e^{hk(1-mI)}},\\
F_{vn} &= \frac{1}{1+e^{-h(P_n-P_v)}} = \frac{1}{1+e^{hk(mI-1)}},\\
F_n^a &= \frac{1}{1+e^{-h(-\omega_n-P_n)}} = \frac{1}{1+e^{h(\omega_n-c_nI)}},\\
F_v^a &= \frac{1}{1+e^{-h(-\omega_v-P_v)}} = \frac{1}{1+e^{h(\omega_v-c_vI-k)}},
\end{aligned}
$$

where h is the selection intensity, $m = (c_n - c_v)/k$ represents the risk threshold at which susceptible individuals decide to switch their strategy through the imitation process and $-\omega_n$ and $-\omega_v$ ($\omega_n, \omega_v > 0$) represent the aspiration level for non-vaccinators and vaccinators, respectively. The aspiration level can be considered a reference point for comparing one's payoff gain. A higher aspiration level means that players are greedy, leading them to revise their strategies when the payoff does not meet their expectations [29]. To prevent the switching probabilities from being consistently greater or less than $1/2$, we impose the following conditions:

$$
m \geq 1, \quad c_n \geq \omega_n \quad \text{and} \quad k \leq \omega_v \leq c_v + k.
$$

2.3. The coupled epidemiological model

Since R_n and R_v do not appear in the other equations, we only need to consider the remaining equations of model (1). The system obtained by coupling the transmission model (1) with the strategy-making model (2) can be described by

$$
\begin{aligned}
\frac{dS_n}{dt} &= (1-p)\mu - \beta_{nn}I_nS_n - \beta_{vn}I_vS_n - \mu S_n,\\
\frac{dS_v}{dt} &= p\mu - \beta_{nv}I_nS_v - \beta_{vv}I_vS_v - \mu S_v,\\
\frac{dI_n}{dt} &= S_n(\beta_{nn}I_n + \beta_{vn}I_v) - \alpha_nI_n - \gamma_nI_n - \mu I_n,\\
\frac{dI_v}{dt} &= S_v(\beta_{nv}I_n + \beta_{vv}I_v) - \alpha_vI_v - \gamma_vI_v - \mu I_v,\\
\frac{dp}{dt} &= \epsilon\xi p(1-p)(F_{nv} - F_{vn}) + \epsilon(1-\xi)[(1-p)F_n^a - pF_v^a].
\end{aligned}
\tag{3}
$$

Since our main interest is the evolutionary dynamics of the pathogen, the infected compartments I_n and I_v play a central role, as they represent infections occurring in non-vaccinated and vaccinated hosts, respectively. A more detailed model could explicitly track the susceptible subgroups S_n and S_v as independent state variables. However, to reduce model dimensionality and focus on pathogen dynamics in the two infectious host types, we introduce a population-level closure approximation for the susceptible classes: $S_v(t) \approx p(t)S(t)$ and $S_n(t) \approx (1-p(t))S(t)$, where $S(t) = S_n(t) + S_v(t)$. This type of approximation is commonly used in models incorporating behavioral change [32,34], and the rationale for its use in the present setting is further discussed in Appendix A. Under this approximation, the behavioral variable $p(t)$, governed by the evolutionary game dynamics, is used to represent the average vaccination composition of susceptible individuals in the reduced model. This yields the following reduced epidemiological-behavioral system:

$$
\begin{aligned}
\frac{dS}{dt} &= \mu - (\beta_{nn}I_n + \beta_{vn}I_v)(1-p)S - (\beta_{nv}I_n + \beta_{vv}I_v)pS - \mu S,\\
\frac{dI_n}{dt} &= (1-p)S(\beta_{nn}I_n + \beta_{vn}I_v) - \alpha_nI_n - \gamma_nI_n - \mu I_n,\\
\frac{dI_v}{dt} &= pS(\beta_{nv}I_n + \beta_{vv}I_v) - \alpha_vI_v - \gamma_vI_v - \mu I_v,\\
\frac{dp}{dt} &= \epsilon\xi p(1-p)(F_{nv} - F_{vn}) + \epsilon(1-\xi)[(1-p)F_n^a - pF_v^a],
\end{aligned}
\tag{4}
$$

where $\epsilon = \tau/t$ is a scaling parameter. The subsequent analysis is mainly based on this reduced epidemiological-behavioral system (4). Consider the region

$$
\mathcal{D} = \{(S, I_n, I_v, p) \in \mathbb{R}_+^4 \,:\, S + I_n + I_v \leq 1,\ p \leq 1\}.
$$

It can be shown that all solutions of system (4) starting in $\mathcal{D}$ remain in $\mathcal{D}$ for all $t \geq 0$. Thus, $\mathcal{D}$ is positively invariant, and it is sufficient to consider solutions in $\mathcal{D}$.

Theorem 1. *The disease-free equilibrium* $E_0 = (1, 0, 0, \bar{p}_0)$ *of system (4) is always feasible and is locally asymptotically stable when* $R_0 < 1$, *where*

$$\bar{p}_0 = \frac{-\tilde{A}_2 - \sqrt{(\tilde{A}_2)^2 - 4\tilde{A}_1\tilde{A}_3}}{2\tilde{A}_1}, \quad R_0 = \frac{\beta_{nn}(1-\bar{p}_0)}{\alpha_n + \gamma_n + \mu} + \frac{\beta_{vv}\bar{p}_0}{\alpha_v + \gamma_v + \mu},$$

with

$$\tilde{A}_1 = -\epsilon\xi\frac{1-e^{hk}}{1+e^{hk}}, \quad \tilde{A}_2 = \epsilon\xi\frac{1-e^{hk}}{1+e^{hk}} - \frac{\epsilon(1-\xi)}{1+e^{h\omega_n}} - \frac{\epsilon(1-\xi)}{1+e^{h(\omega_v-k)}}, \quad \tilde{A}_3 = \frac{\epsilon(1-\xi)}{1+e^{h\omega_n}}.$$

Proof See Appendix B.

Here, R_0 is the basic reproduction number of system (4), which denotes the expected number of secondary infections produced in a completely susceptible population by a single infected individual during his/her infectious period [35]. Specifically, when the entire population adopts the non-vaccination (resp., vaccination) strategy, we set $p = 0$ (resp., $p = 1$). In this case, model (4) reduces to a three-dimensional system; that is, the dynamics of I_v (resp., I_n) are not taken into account. A straightforward computation yields the resulting basic reproduction number, denoted by R_{0n} (resp., R_{0v}), where

$$R_{0n} = \frac{\beta_{nn}}{\alpha_n + \gamma_n + \mu}, \quad R_{0v} = \frac{\beta_{vv}}{\alpha_v + \gamma_v + \mu}.$$

We next prove the persistence of system (4) for $R_0 > 1$ by applying standard methods [36], shown in the following theorem (see Appendix C for details).

Theorem 2. *If* $R_0 > 1$, *there exists a positive constant* $\eta \in (0, 1)$ *such that for the system (4)*

$$\liminf_{t\to\infty}(S(t), I_n(t), I_v(t), p(t)) \geq (\eta, \eta, \eta, \eta), \tag{5}$$

with the initial conditions $(S(0), I_n(0), I_v(0), p(0)) \in \mathrm{Int}\mathcal{D}$, *where* η *is independent of initial conditions in* $\mathrm{Int}\mathcal{D}$.

The threshold R_0 determines whether the disease will die out. In the case where vaccination affects only the transmission rate β, incorporating multiple strategy-adjustment mechanisms lowers the disease-elimination threshold compared with the non-vaccination model (i.e., $R_0 < R_{0n}$), thereby facilitating disease eradication. This shows that the adoption of vaccination is conducive to disease control. However, this threshold remains higher than that corresponding to universal vaccination in the population; i.e., $R_0 > R_{0v}$.

Under voluntary vaccination and imperfect vaccine assumptions, numerical simulation further shows that the coupled epidemiological model (4) can induce sustained oscillations via a Hopf bifurcation (see Fig. 2(a)), as demographic turnover (birth/death) supplies susceptibles and thus promotes the persistence of these cycles. This implies that, unless specific conditions are met, voluntary vaccination alone is insufficient to eliminate disease spread, a conclusion that aligns with the findings in [3]. Since the transmission dynamics (1) and the strategic vaccination process (2) may operate on distinct time scales, we introduce a scaling parameter ϵ to characterize this separation. Here, $\epsilon = \tau/t$, with smaller values of ϵ corresponding to hesitant vaccination decision-making. As indicated by the bifurcation structure in Fig. 2(b), ϵ serves as the key control parameter inducing a Hopf bifurcation; in particular, oscillations are suppressed only when the strategy-updating process is sufficiently slow (i.e., $\epsilon < 0.026$). When $0 < \epsilon \ll 1$, p acts as a slow variable, and the dynamics of the coupled model (4) resemble those of the classical SIR epidemic model. It should be noted that system (3) could yield a bifurcation structure similar to that shown in Fig. 2(b), as illustrated in Fig. A.1(d). This further indicates that the reduced system captures the qualitative dynamical behaviour of system (3).

In conclusion, our results demonstrate that the inclusion of strategy dynamics modifies the disease-elimination threshold and can lead to the emergence of periodic solutions, which are not observed in the classical epidemiological model without strategy change. In what follows, we establish evolutionary dynamics for pathogen virulence to study its evolution in the presence of vaccination.

3. Evolutionary adaptation in mean pathogen virulence

Next, we focus on the evolution of the pathogen's mean virulence level $\bar{V}_j$ ($j \in \{n, v\}$), a phenotypic trait. In the framework developed below, our analysis is confined to scenarios in which the disease persists ($R_0 > 1$; see Theorem 2), employing a combined aspiration- and imitation-based updating rule. For the sake of simplicity, we do not consider multiple infections. Assume that the distribution of V_j in the population is concentrated around the population mean $\bar{V}_j$. Further, suppose that both the transmission rates and disease-induced mortality are increasing functions of virulence, reflecting a trade-off between enhanced transmissibility and reduced host survival, where

$$\begin{aligned} &\beta_{nn} \approx \theta_n\beta(\bar{V}_n), \quad \beta_{vn} \approx \theta_n\beta(\bar{V}_v), \quad \alpha_n \approx \alpha(\bar{V}_n), \\ &\beta_{vv} \approx \theta_v\beta(\bar{V}_v), \quad \beta_{nv} \approx \theta_v\beta(\bar{V}_n), \quad \alpha_v \approx \alpha(\bar{V}_v). \end{aligned} \tag{6}$$

Without loss of generality, we assume $\theta_n = 1$ as the baseline host susceptibility and denote $\theta = \theta_v \in (0, 1)$. Here, θ reflects the reduction in infectious potential resulting from vaccination. If β and α are linear in $\bar{V}_j$, then "≈" in Approximation (6) can be replaced by " = ". To simplify the analysis, we assume the recovery rate remains constant, as its evolution involves host defenses, which are beyond the scope of this study, but which we have previously investigated [12].

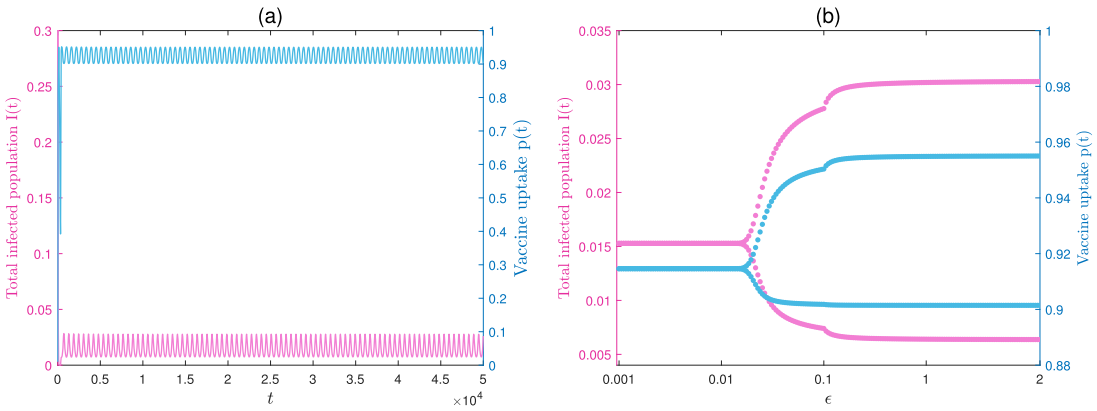

Fig. 2. An illustration of population oscillations driven by the evolving vaccination strategy in the absence of pathogen evolution. (a) Time series curves obtained though simulation of (4) with $\epsilon = 0.1$. (b) Bifurcation diagram of the total infected population $I(t)$ and the vaccine uptake $p(t)$ with respect to the scaling parameter ϵ. The remaining parameter values are $\mu = 0.002$, $\beta_{nn} = 0.375$, $\beta_{vn} = 0.1875$, $\beta_{vv} = 0.119$, $\beta_{nv} = 0.238$, $\alpha_n = 0.02$, $\alpha_v = 0.015$, $\gamma_n = 0.05$, $\gamma_v = 0.05$, $\xi = 0.9$, $h = 500$, $k = 0.001$, $c_n = 1.5$, $c_v = 0.5$, $\omega_n = 0.001$ and $\omega_v = 0.005$. The initial values are $(S(0), I_n(0), I_v(0), p(0)) = (0.9, 0.09, 0.01, 0.01)$.

Assuming the mutation rate is negligible, the evolutionary dynamics can be derived following [10,18] as

$$\begin{aligned}\frac{d\bar{V}_n}{dt} &= G_n\left(\beta'(\bar{V}_n)(1-p)S - \alpha'(\bar{V}_n)\right) + G_v\frac{I_v}{I_n}(1-p)S\beta'(\bar{V}_v) + \frac{I_v}{I_n}(1-p)S\beta(\bar{V}_v)(\bar{V}_v - \bar{V}_n),\\ \frac{d\bar{V}_v}{dt} &= G_v\left(\theta\beta'(\bar{V}_v)pS - \alpha'(\bar{V}_v)\right) + G_n\frac{I_n}{I_v}\theta pS\beta'(\bar{V}_n) + \frac{I_n}{I_v}\theta pS\beta(\bar{V}_n)(\bar{V}_n - \bar{V}_v),\end{aligned} \tag{7}$$

where G_n and G_v represent the evolutionary adaptation rates in strain types among naïve and vaccinated hosts, respectively (see Appendix D for details). For simplicity, we assume G_n and G_v are constant. System (7) captures the effects of selection (first term), selection within the migrant pool (second term) and migration (third term) on the evolution of the mean virulence.

In line with previous theoretical studies on virulence evolution [10,11,37], our results are based on a positive correlation between transmissibility and disease-induced mortality, characterized by an increasing and saturating transmission-virulence function together with an increasing mortality-virulence function. More specifically, we use the functional form

$$\beta(\bar{V}_j) = \frac{\beta_0\bar{V}_j^2}{1 + h_v\bar{V}_j^2}, \quad \alpha(\bar{V}_j) = \alpha_0\bar{V}_j^2 \tag{8}$$

in all our simulations. Here, β_0 is the baseline transmission rate and α_0 is the baseline disease-induced mortality, while h_v is a dimensionless positive constant.

Theorem 3. *Consider model (7) with any initial condition* $(\bar{V}_n(0), \bar{V}_v(0)) \in \mathbb{R}^2_+$. *The solution* $(\bar{V}_n(t), \bar{V}_v(t))$ *remains nonnegative for all* $t \geq 0$. *Further, the solution is bounded in* $\mathbb{R}^2_+$.

Proof. See Appendix E.

It is worth noting that systems (4) and (7) characterize the coupled evolutionary-epidemiological dynamics under a dynamic vaccination strategy, which will be further analysed below.

3.1. Numerical continuation of the long-term effects of the evolutionary adaptation

3.1.1. Effects of evolutionary adaptation rates on oscillation amplitude

We now analyze the influence of the adaptation rate G_j on the coupled evolutionary-epidemiological system's dynamical behaviour. Specifically, we restrict our attention to the case in which the two infected groups exhibit identical adaptation rates ($G_n = G_v = G$). From Figs. 3 and 4, it can be observed that as G increases, the amplitudes of both the infected population and trait cycles vary in a non-monotonic manner. As the evolutionary rate G gradually increases, the system undergoes distinct phases, as detailed below.

(I) Population cycle phase

When the adaptation rate G is extremely small, the infected population I and the vaccine uptake p exhibit periodic oscillations with an approximately constant amplitude, while the mean trait value $\bar{V}_j$ remains nearly stationary in this phase, with an amplitude smaller than 0.0001 (see Fig. 3). In this phase, evolution cannot keep pace with the epidemiological changes, and the population dynamics are therefore mainly governed by epidemiological interactions. Despite their large amplitude, the population fluctuations in this phase are predictable, since the dynamics are effectively governed by low-dimensional epidemiological ODEs with negligible evolutionary feedback.

(II) Trait-population cycle phase

When the adaptation rate G becomes large, the amplitude of the oscillations in $\bar{V}_j$ increases markedly with an amplitude between 0.0001 and 0.01, whereas that of the infected population I becomes slightly smaller (see Fig. 3). This is because we consider the evolution of the pathogen; in this case, the direction of evolution is expected to maximize the pathogen's fitness [11]. Therefore, the system represents an eco-evolutionary framework with a stabilizing evolutionary feedback. Although an intermediate evolutionary rate enables trait changes to exert significant feedback on epidemiological dynamics, such evolutionary changes cannot immediately alleviate population oscillations because of a timescale mismatch between epidemiological fluctuations and evolutionary response. This "evolutionary lag effect" results in only partial buffering of population fluctuations, which therefore remain pronounced. Note that in this phase, p oscillates with an approximately constant amplitude, indicating that the vaccine uptake is less sensitive to variations in the adaptation rate than the infected population I. This is reasonable, as the pathogen influences vaccine uptake indirectly through its impact on the infected population.

(III) Cryptic Red Queen dynamics phase

When the adaptation rate G becomes even larger, the amplitude of oscillations in the mean trait $\bar{V}_j$ becomes larger with an amplitude exceeding 0.01, whereas a pronounced reduction in the oscillation amplitude of the infected population density I and the vaccine uptake p is observed (see Fig. 3). In this phase, the rapid adaptation rate allows the trait to respond quickly, resulting in seemingly small fluctuations in macro-level population density but intense underlying evolutionary dynamics. This reflects a dynamic where the stability of large-scale population dynamics may necessitate substantial evolutionary changes at the micro level for its maintenance. Moreover, small-scale evolutionary processes do not always translate into large-scale population changes, highlighting the complex interplay between individual adaptations and population-level dynamics. We therefore refer to this regime as the 'cryptic red queen dynamics' phase [38].

(IV) Stationary phase

When the adaptation rate exceeds a threshold, oscillations in both population size and trait value vanish entirely (see Fig. 3). This suggests that, in a non-closed population with a continuous influx of susceptible individuals, rapid adaptation rates facilitate the stabilization of both the macroscopic population and the underlying microscopic traits [38].

Mathematically, Fig. 3 depicts bifurcation diagrams with respect to G, which serves as the bifurcation parameter. Moreover, adopting the parameter set from Fig. 3, we use MATCONT to construct the bifurcation diagrams of variables I_n, I_v, V_n and V_v as functions of G (see Fig. F.1 in Appendix F). Fig. F.1 shows that the coupled evolutionary system exhibits a Hopf bifurcation (denoted H, when $G = 0.0583$) at the interface between the cryptic Red Queen dynamics phase and the stationary phase. As G decreases below 0.0583, the epidemic equilibrium (EE) loses stability via this Hopf bifurcation, and numerical simulations indicate the existence of a locally stable limit cycle surrounding the EE for $0 \leq G < 0.0583$.

Further, we observe two distinct patterns in the amplitude of trait cycles: the amplitudes either reach a peak at an intermediate adaptation rate before abruptly stabilizing above a threshold (see Fig. 3) or they increase with G (see Fig. 4). In this case, as the adaptation rate increases, the macroscopic population exhibits cyclic oscillations with an approximately constant amplitude, while at the microscopic level, the amplitude of trait fluctuations gradually increases. This phenomenon further highlights the complex interplay between individual adaptation and population-level dynamics.

In the preceding discussion, we assumed that the evolutionary adaptation rate was identical in the naïve and vaccinated groups ($G_n = G_v$). We also extended the analysis to the case where the evolutionary rates differed between the two groups ($G_n \neq G_v$; see Figs. G.1 and G.2 in Appendix G). We found that when the evolutionary adaptation rates of the two groups are not substantially different, so the dynamics resemble those illustrated in Figs. 3 and 4. However, when G_n and G_v differ substantially, the situation becomes more complex. For instance, the stationary phase is more likely to occur in the vicinity of $G_n \approx 0.1$ (see Fig. G.1).

3.1.2. The impact of vaccine-induced transmission blocking on the epidemic steady states

The transmissibility of a viral strain serves as a key indicator for evaluating a vaccine's performance against that focal strain. We assume the vaccination to be primarily aimed at blocking transmissibility of the focal strain. Define the vaccine-induced transmission-blocking efficacy (VTE) as the reduction in transmissibility that vaccination confers, given by VTE $= 1 - \theta \in (0, 1)$. Given the current lack of knowledge regarding the functional relationship among vaccination efficacy, virulence and recovery rate, we examine three possible scenarios for the recovery rate: $\gamma_v > \gamma_n$, $\gamma_v = \gamma_n$ and $\gamma_v < \gamma_n$ (as shown in Fig. 5).

As illustrated in Fig. 5(a), I^* declines monotonically with increasing VTE, whereas p^* exhibits a non-monotonic pattern, attaining its maximum at around VTE ≈ 0.8. This shows that when the VTE becomes sufficiently high, further enhancement of vaccine efficacy may result in a decrease in the equilibrium vaccine uptake p^*, which reflects the population's autonomous decision-making behaviour. This is reasonable, since the perceived risk of infection is greatly reduced as VTE becomes high, making susceptible individuals less willing to bear the potential risks associated with vaccination and thus less inclined to be vaccinated. However, as VTE continues to increase, even though the equilibrium vaccine uptake p^* decreases, the steady-state density of total infected individuals I^* still declines. This demonstrates that enhancing vaccine effects remains an effective strategy for disease control. It is noteworthy that only when vaccine efficacy is sufficiently high will the density of unvaccinated infected individuals (I_n^*) begin to decline (see Fig. 5(b)). Furthermore, we find that a higher recovery rate among vaccinated individuals ($\gamma_v > \gamma_n$ scenario) leads to increased vaccine uptake in the population and consequently mitigates disease transmission (see the red solid curves in Fig. 5(a)–(b)).

As the pathogen undergoes continuous evolution, the equilibrium virulence dynamically responds to increasing VTE. Importantly, we find that even when the naïve population remains unvaccinated, the equilibrium virulence $\bar{V}_n^*$ still varies with VTE (see Fig. 5(c)). For the convenience of analysis, we fix the recovery γ_n. From Fig. 5(c), it can be observed that when $\gamma_v = \gamma_n$, the equilibrium virulence values satisfy $\bar{V}_v^* \approx \bar{V}_n^*$, and their dependence on VTE becomes negligible, with $\bar{V}_j^*$ remaining nearly constant.

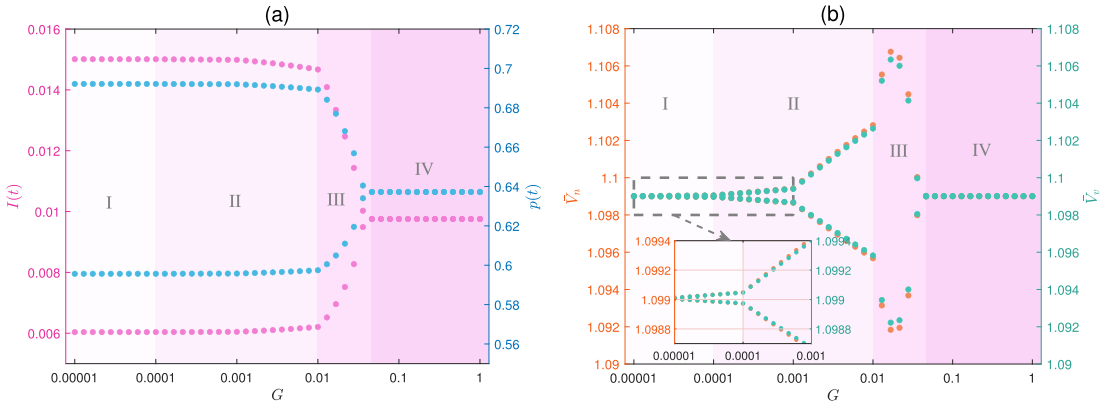

Fig. 3. Bifurcation diagrams of (a) infectious density I and vaccine uptake p, and (b) mean trait dynamics $\bar{V}_j$ in relation to the speed of adaptation G (when $G = G_n = G_v$). We observe four distinct phases: the population cycle phase (I), the trait-population cycle phase (II), the cryptic Red Queen dynamics phase (III), and the stationary phase (IV). The pink-shaded regions correspond to these three phases in progressively darker tones. The remaining parameter values are $\mu = 0.004$, $\theta = 0.4$, $\gamma_n = 0.12$, $\gamma_v = 0.12$, $\epsilon = 0.01$, $\xi = 0.1$, $h = 500$, $k = 0.001$, $c_n = 1.5$, $c_v = 0.5$, $\omega_n = 0.001$, $\omega_v = 0.005$, $\beta_0 = 1.5$, $\alpha_0 = 0.085$ and $h_v = 1$.

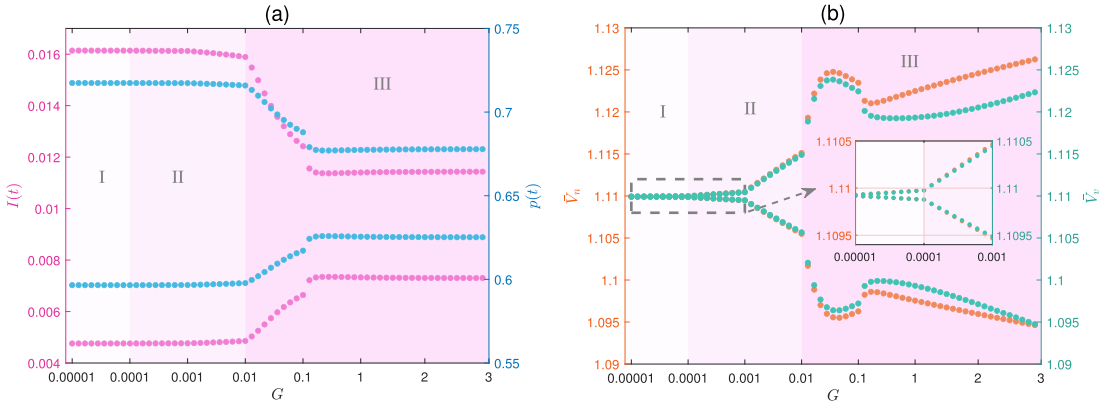

Fig. 4. Bifurcation diagrams of (a) infectious density I and vaccine uptake p, and (b) mean trait dynamics $\bar{V}_j$ in relation to the speed of adaptation G (when $G = G_n = G_v$). The shaded areas in the panels indicate the different phases shown in Fig. 4 but without the stationary phase. We set $\gamma_n = \gamma_v = 0.125$, and the remaining parameter values are as in Fig. 3.

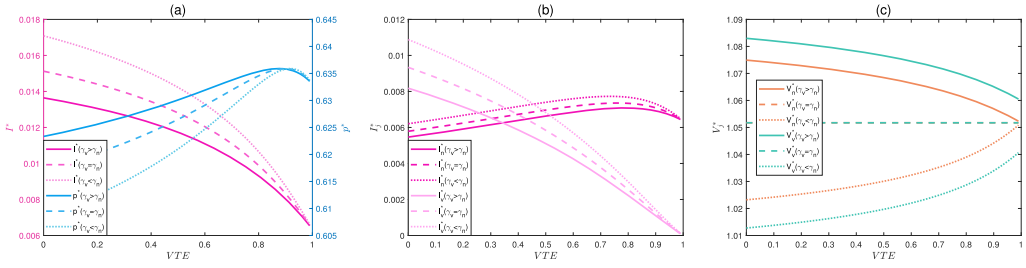

Fig. 5. Equilibrium variation in (a) total infectious density I^* and vaccine uptake p^*, (b) infectious densities I_j^* and (c) mean trait value $\bar{V}_j$, under varying VTE. For $\gamma_v > \gamma_n$ case, we choose $\gamma_v = 0.12$; for $\gamma_v < \gamma_n$ case, we choose $\gamma_v = 0.08$. Parameter values are $\mu = 0.004$, $\alpha_0 = 0.085$, $\epsilon = 0.1$, $\xi = 0.1$, $h = 150$, $k = 0.001$, $c_n = 1.5$, $c_v = 0.5$, $\omega_n = 0.001$, $\omega_v = 0.005$, $\beta_0 = 1.5$, $h_v = 1$, $G_n = 0.1$, $G_v = 0.1$ and $\gamma_n = 0.1$. Remaining parameters are as in Fig. 4.

When $\gamma_v > \gamma_n$, the equilibrium virulence levels $\bar{V}_j^*$ exhibit a decline as VTE increases, with $\bar{V}_v^* > \bar{V}_n^*$ across the range of VTE. In contrast, when $\gamma_v < \gamma_n$, both equilibrium virulence levels $\bar{V}_n^*$ and $\bar{V}_v^*$ increase with growing VTE, and the ordering reverses such that $\bar{V}_v^* < \bar{V}_n^*$. Notably, increasing the recovery rate of vaccinated hosts drives an overall increase in pathogen virulence. This suggests that when the recovery rate is relatively low, the pathogen could evolve to increase its virulence to compensate for losses due to host clearance and vaccination. However, as the recovery rate further increases, pathogens become unable to offset the reduction in infected hosts by elevating virulence, making higher virulence an unfavourable evolutionary strategy. This conclusion is consistent with previous studies [12].

4. Pathogen evolution during vaccination campaigns

The above analysis investigated the steady state of the coupled evolutionary-epidemiological system, yielding the final vaccine uptake and the equilibrium proportions of each subpopulation. We restricted our attention to the evolution of the mean virulence of the circulating pathogen in the population in the previous analysis. However, multiple strains may coexist during the vaccination period, and new variants might emerge persistently. The main objective of this section is to analyze the evolutionary direction of strain types, with a particular focus on potential immunity-adapted variants—that is, those that are well adapted to vaccine-induced immunity—since such variants can pose substantial risks. In this section, we restrict our analysis to the case during (or at the early stage of) vaccination.

4.1. Conceptualizing variant evolution

Pathogen adaptation to naïve and vaccinated hosts depends on the emergence of new variants and their fitness within each host type [9]. Adaptation can be quantified by considering both the absolute per capita growth rate of infections caused by a variant and also this rate relative to that of the currently dominant (wild-type) strain. The former determines if the variant can spread in a population, whereas the latter will determine if the variant can increase in frequency and thereby potentially replace the currently dominant type [9].

For a variant i to spread in a population, its absolute growth rate f^i must be positive ($f^i > 0$). We regard f^i as the fitness of variant i. To increase in relative frequency, its selection coefficient s, defined as the difference between its growth rate and that of the wild type, must also be positive ($s > 0$). The fitness f^i of any pathogen variant i and its selection coefficient s can be approximated as follows (see Appendix H for details)

$$f^i = (1-p)f_n^i + pf_v^i, \tag{9}$$

with

$$f_n^i = \beta_{nn}^i S - \alpha_n^i - \gamma_n^i - \mu, \quad f_v^i = \beta_{vv}^i S - \alpha_v^i - \gamma_v^i - \mu,$$

where f_n^i and f_v^i are the fitnesses of variant i in fully naïve and vaccinated hosts, respectively. We have

$$s = (1-p)\Delta f_n + p\Delta f_v, \tag{10}$$

where Δf_n and Δf_v are the differences in fitness between the mutant (m) and the wild type (w) in fully naïve ($p = 0$) and fully vaccinated ($p = 1$) populations, respectively. It is worth noting that $f_n^i > 0$ (resp., $f_v^i > 0$) if and only if the effective reproduction number $R_{0n}^i(t)$ in a fully naïve (resp., $R_{0v}^i(t)$ in a fully vaccinated) host population exceeds unity, assuming that only strain i is circulating.

With this setup, we can provide a precise definition of a variant being adapted to vaccinated or naïve host populations. Since vaccines are developed against the currently dominant strain (the wild type), we focus exclusively on immunity-adapted variants; i.e., those for which $\Delta f_v > 0$. These immunity-adapted variants are more fit than the wild type in a fully vaccinated population and therefore pose a heightened threat to public health. We classify these immunity-adapted variants by their fitness and selection coefficient following [9], a categorization that is specific to immunological context.

From a selection coefficient perspective, we classify these immunity-adapted variants as either generalists or specialists. An immunity-adapted variant with $\Delta f_n > 0$ is termed a “generalist", as it spreads better than the wild type in both naïve and vaccinated hosts; whereas if $\Delta f_n < 0$, it is termed a “specialist", being fitter only in vaccinated hosts. From a fitness perspective, immunity-adapted variants are classified as immunity-inhibited or immunity-facilitated: the former’s fitness decreases as the fraction of the vaccinated population rises ($df^i/dp < 0$), while the latter’s fitness increases ($df^i/dp > 0$). This categorization indicates how vaccination and immunity-driven pathogen evolution affect infection spread. During vaccination campaigns, emerging variants can be either specialists or generalists, and either immunity-inhibited or immunity-facilitated [9].

4.2. A case study

We first examine the evolutionary trajectory of the wild-type phenotype, $\beta_{jz}^w = \theta_z\beta(V_j^w)$ and $\alpha_j^w = \alpha(V_j^w)$, by analyzing the evolution of the wild-type virulence V_j^w, where $j, z \in \{v, n\}$. The phenotypic trait of the dominant strain V_j^w approaches the mean trait $\bar{V}_j$, and we approximate the dynamics of V_j^w by system (7). Accordingly, we derive the fitness values f_n^w and f_v^w of the wild-type strain in fully naïve and fully vaccinated hosts, respectively. We focus on the early phase of vaccination, during which the vaccine uptake is still low and the proportion of susceptible individuals in the population remains nearly constant.

To further exhibit the direction of immunity-adapted pathogen types, we parameterize systems (4) and (7) using daily reported number of new positive COVID-19 cases in Tokyo from June 12, 2022, to March 18, 2023. This dataset is obtained from [32]. During the selected period, we assume that the actual daily incidence is approximately fivefold higher than the reported positive cases [32] and compute the corresponding weekly proportion of newly infected individuals (see circle markers in Fig. 6(b)). In this study, we focus on short-term data and assume an average recovery period of one week. Accordingly, we set $\mu = 0$ and $\gamma_n = \gamma_v = 0.1429$ as in [32]. We employ the Least Squares Method to fit the parameters; the fitting results are shown in Fig. 6(b). We obtain a coefficient of determination of $r^2 = 0.8554$, which suggests that the model provides a satisfactory fit to the data. The fitted value of ξ is 0.8554, indicating that imitation mechanism played a prominent role in the strategy-updating process at this stage of the pandemic.

The magnitude of the partial rank correlation coefficients (PRCCs) shows the sensitivity of these parameters and the sign of the PRCCs indicates the positive or negative relationship between the inputs (estimated parameters) and outputs (the cumulative number of infected individuals). Due to limited information on the distribution of each parameter, we adopt a uniform distribution for all input parameters x, as proposed in [39]. The ranges for each parameter are defined as $[x-3\delta, x+3\delta]$, following the 3δ principle, with the mean set equal to its fitted value (see Fig. 6). The results show that the baseline transmission rate β_0, which is directly related to disease transmission, has the greatest impact on the cumulative number of infections, followed by the imitation emphasis parameter ξ (see Fig. 6(c)). This further confirms that the imitation mechanism played a prominent role in the strategy-updating process during the early stage of the pandemic.

We analyze the first 14 weeks and obtain the weekly fitness coordinates $(f_v^w(t), f_n^w(t))$ at $t = 0$, 7 and 14 weeks (blue dots, Fig. 7). Numerical simulations also show that, during this period, the vaccine uptake increases over time. However, the specific phenotype of a variant V_j^m cannot be known in advance. Since the mutation is small, we therefore treat the fitness of a variant f_j^m as random variables that fluctuate around f_j^w $(j \in n, v)$. In the numerical simulations, we assume that f_j^m follows a Gaussian distribution with mean f_j^w and variance 0.3 (black dots, Fig. 7). Note that we do not consider the evolution of these variants, nor do we account for interactions among different variant strains, as this is too complex and beyond the scope of this study. Therefore, the black dots remain unchanged between Fig. 7(a)–(b) and serve merely as a schematic illustration.

In the early phase of the host–pathogen association, the vaccine uptake p is low, and the unvaccinated population remains relatively large. Consequently, most potential new variants are expected to adapt to both host types n and v, meaning that they are more likely to be generalists. As shown in Fig. 7(a), the purple region is relatively large, and many of the black dots tend to fall within this region. Over time, as vaccine uptake increases and the proportion of vaccinated individuals in the population rises, most potential variants are expected to adapt primarily to v-type hosts, and there will be fewer variants that increase fitness in both host types, implying a higher likelihood of these variants being specialists for further adaptation. As a pathogen becomes progressively adapted to a novel host, further adaptation to vaccinated hosts is likely to occur at the expense of some degree of adaptation to non-vaccinated hosts [9]. From Fig. 7(b), we observe that the yellow region expands, with most variants falling within it. Furthermore, the immunity-maladapted region also enlarges, indicating that the increase in vaccine uptake is more conducive to limiting the emergence of harmful variants. In general, if SARS-CoV-2 undergoes further adaptation in response to immune priming, our results suggest that the long-term evolutionary outcome is likely to favour the emergence of specialist variants, in line with the findings of Day et al. [9]. It is worth noting that, unlike previous studies, our framework incorporates game-theoretic strategic dynamics and quantitatively characterizes evolutionary directions, rather than presenting merely illustrative evolutionary diagrams. In addition, we calibrate the model with real epidemic data.

5. The simplified evolutionary-epidemiological system

In the above analysis, we considered the pathogen's trait (virulence) to vary across host types. Next, we discuss the case in which the pathogen trait does not vary between host types; that is, $\bar{V} = \bar{V}_n = \bar{V}_v$. With respect to the evolutionary dynamics of the mean virulence, the migration force between host types no longer needs to be taken into consideration. In this scenario, vaccination affects the host susceptibility θ, and the infected population can therefore be treated as a single class I. Since vaccination games driven by imitation dynamics have been shown to capture real-world behaviour to a large extent [3,25], we restrict our attention to vaccination games based on the imitation mechanism to simplify the model analysis. We extend the classic vaccination-game dynamic model [3], and the resulting simplified evolutionary-epidemiological system is given by

$$\begin{aligned}
\frac{dS}{dt} &= \mu - (1-p+\theta p)\beta(\bar{V})SI - \mu S,\\
\frac{dI}{dt} &= (1-p+\theta p)\beta(\bar{V})SI - \alpha(\bar{V})I - \gamma I - \mu I,\\
\frac{dp}{dt} &= \epsilon k \rho p(1-p)(mI-1),\\
\frac{d\bar{V}}{dt} &= G((1-p+\theta p)\beta'(\bar{V})S - \alpha'(\bar{V})),
\end{aligned} \tag{11}$$

where ρ represents the combined imitation rate at which individuals sample others and switch strategies [3]. We adopt the same nonlinear trade-off forms as in (8). Since $\beta'(\bar{V}) < \beta_0/\sqrt{h_v}$, we have $d\bar{V}/dt \le 2G(\beta_0/\sqrt{h_v} - \alpha_0 v)$. By exploiting the comparison principle, we have $\lim\limits_{t\to\infty} \sup \bar{V}(t) \le \beta_0/(\alpha_0\sqrt{h_v})$. Let

$$\mathcal{D}_s = \{(S, I, p, \bar{V}) \in \mathbb{R}_+^4 : S + I \le 1,\ p \le 1,\ \bar{V} \le \frac{\beta_0}{\alpha_0\sqrt{h_v}}\},$$

which is a positively invariant set of the simplified system (11). In the following, we focus on the feasibility and stability of the possible equilibria of the simplified evolutionary-epidemiological system (11). Direct computation yields the following results.

Theorem 4. *The simplified system (11) has up to seven equilibria:*
(1) Two disease-free, pure non-vaccinator equilibria, $E_{01}^n = (1,0,0,0)$ *and* E_{02}^n*, where*

$$E_{02}^n = (1,0,0,v_0^n) = \left(1,0,0,\left(\frac{\sqrt{\beta_0}-\sqrt{\alpha_0}}{h_v\sqrt{\alpha_0}}\right)^{\frac{1}{2}}\right).$$

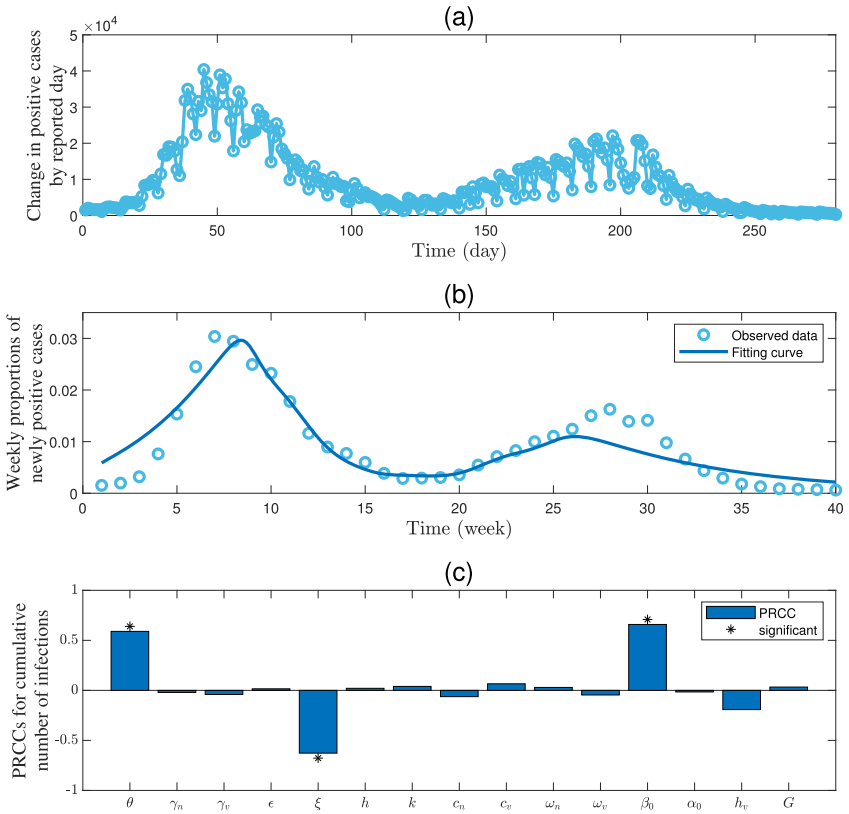

Fig. 6. (a) Change in positive COVID-19 cases by reported day in Tokyo from June 12, 2022, to March 18, 2023. (b) Weekly proportions of newly positive cases (circle markers) and the corresponding model fitting results (solid line). (c) Sensitivity analysis: PRCC value for cumulative number of infections over 40 weeks based on system (4) and (7) with respect to estimated parameters. The sample size is set to 1000 and (*) denotes PRCCs that are significant. We set $\mu = 0$ and $\gamma_n = \gamma_v = 0.1429$ (values from [32]). The estimated parameter values are $\theta = 0.75$, $\epsilon = 3$, $\xi = 0.811$, $h = 100.0215$, $k = 0.0674$, $c_n = 2.4764$, $c_v = 1.9449$, $\omega_n = 0.1932$, $\omega_v = 0.2971$, $\beta_0 = 0.95$, $\alpha_0 = 0.1028$, $h_v = 1.0305$ and $G_n = G_v = 0.2086$, with initial conditions $S(0) = 0.975$, $I_n(0) = 0.02$, $I_v(0) = 0.005$, $p(0) = 0.02$, $V_n(0) = 0.6$ and $V_v(0) = 0.6$.

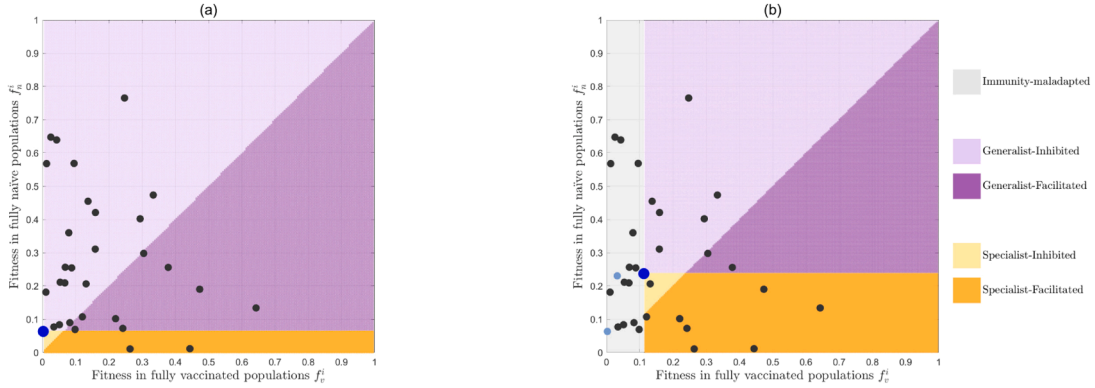

Fig. 7. The direction of pathogen immunity-adapted types. Plots of the fitness of possible variants in a fully naïve and a fully vaccinated population (dots). The blue dots indicate the prevailing wild type; i.e., the dominant strain with the highest fitness. The black dots indicate the possible variants. Variants in the grey region are immunity-maladapted ($\triangle f_v < 0$). The shaded regions indicate the four different kinds of variants. (a) Early phase of the host–pathogen association: the large blue dot denotes the wild type at $t = 0$ ($p = 0.02$). (b) Later phase of the association: the large blue dot denotes the wild type at $t = 14$ weeks ($p = 0.8178$). The successive light blue dot denotes the wild type at $t = 7$ ($p = 0.0778$) weeks. Parameters are as in Fig. 6.

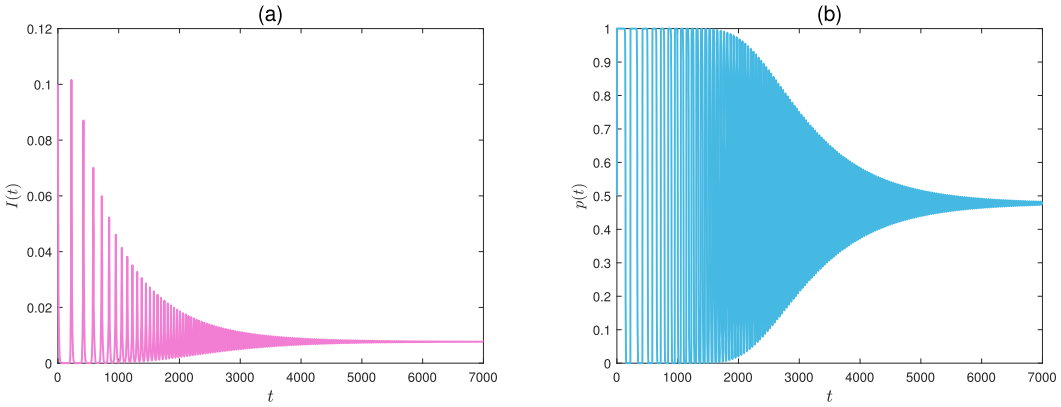

Fig. 8. Time series in (a) total infected population and (b) vaccine uptake. Parameter values are $\mu = 0.005$, $\alpha_0 = 0.05$, $\epsilon = 1$, $x = 0.4$, $h_v = 1.2$, $k = 1.3$, $m = 130$, $\beta_0 = 0.8$, $G = 0.02$, $\gamma = 0.11$ and $\theta = 0.2$.

The equilibrium E_{01}^n always exists, whereas E_{02}^n exists provided that $\beta_0 > \alpha_0$.
(2) Two disease-free, pure vaccinator equilibria, $E_{01}^v = (1, 0, 1, 0)$ and E_{02}^v, where

$$E_{02}^v = (1, 0, 1, v_0^v) = \left(1, 0, 1, \left(\frac{\sqrt{\theta\beta_0} - \sqrt{\alpha_0}}{h_v\sqrt{\alpha_0}}\right)^{\frac{1}{2}}\right).$$

The equilibrium E_{01}^v always exists, whereas E_{02}^v exists provided that $\theta\beta_0 > \alpha_0$.
(3) Three endemic equilibria: a pure non-vaccinator equilibrium $E_n^* = (S_n^*, I_n^*, 0, v^*)$, a pure vaccinator equilibrium $E_v^* = (S_v^*, I_v^*, 1, v^*)$ and a mixed endemic equilibrium $E^* = (S^*, I^*, p^*, v^*)$ corresponding to coexistence of the two strategies. The equilibrium E_n^* exists provided that $R_c > 1$; E_v^* exists provided that $\theta R_c > 1$; and E^* exists provided that $(1 - p^* + \theta p^*)R_c > 1$ and $m \in (m_b, m_t)$. Here,

$$S_n^* = \frac{1}{R_c},\ S_v^* = \frac{1}{\theta R_c},\ S^* = \frac{1}{(1 - p^* + \theta p^*)R_c},\ I_n^* = \mu\frac{R_c - 1}{\beta(v^*)},\ I_v^* = \mu\frac{\theta R_c - 1}{\theta\beta(v^*)},\ I^* = \frac{1}{m},$$

$$p^* = \frac{m\mu\beta(v^*) - (\alpha(v^*) + \gamma + \mu)(\beta(v^*) + m\mu)}{(1 - \theta)\beta(v^*)(m\mu - (\alpha(v^*) + \gamma + \mu))},\ v^* = \left(\frac{\gamma + \mu}{\alpha_0 h_v}\right)^{\frac{1}{4}},$$

$$R_c = \frac{\beta(v^*)}{\alpha(v^*) + \mu + \gamma}\ m_b = \frac{1}{I_n^*},\ m_t = \frac{1}{I_v^*}.$$

Next, we provide results on the stability of these equilibria.

Theorem 5.

1. *E_{01}^n is globally asymptotically stable if $\beta_0 < \alpha_0$. For $\beta_0 > \alpha_0$, E_{02}^n is globally asymptotically stable if $R_g^n < 1$, where $R_g^n = \beta(v_0^n)/(\alpha(v_0^n) + \mu + \gamma)$.*
2. *E_{01}^v and E_{02}^v are always unstable.*
3. *For $R_c > 1$, E_n^* is locally asymptotically stable if $m < m_b$. For $\theta R_c > 1$, E_v^* is locally asymptotically stable if $m > m_t$. E^* is locally asymptotically stable whenever it exists.*

Note that $R_g^n > 1$ if and only if $R_c > 1$ when $\beta_0 > \alpha_0$.

Proof. See Appendix I.

The local asymptotic stability of E^* excludes the possibility of a stable cycle bifurcating from this equilibrium. Notably, the disease incidence could undergo long transient oscillations before approaching the endemic equilibrium (see Fig. 8). The virulence of a competitive pathogen should remain positive even when infections are nearly absent, thereby allowing the disease to spread in the initial phase of an epidemic. This implies that the threshold R_g^n represents the basic reproduction number of the disease in a fully non-vaccinated population [11]. Unlike previous studies, we incorporate the evolutionary dynamics of pathogen virulence into the vaccination model. As both the transmission rate β and the disease-induced mortality α are explicit functions of virulence $\bar{V}$, the classical threshold R_0 governing disease extinction is consequently modified. Here, there exist two thresholds, $R_g^n(v_0^n)$ and $R_c(v^*)$ with $R_g^n \neq R_c$. Since $R_g^n(v_0^n) > 1$ holds true if and only if $R_c(v_0^n) > 1$, the threshold condition for controlling disease extinction is essentially unique. In the absence of pathogen evolution, these two thresholds coincide; that is, $R_0 = R_g^n = R_c$.

From the explicit expression of p^*, it follows that p^* is a monotonically decreasing function of VTE $= 1 - \theta$. In contrast, models incorporating both aspiration-based and imitation-based updating rules provide a more realistic description of decision-making dynamics: as VTE increases, p^* first increases and then decreases, as illustrated in Fig. 5(a). Furthermore, the expression of v^* implies that v^* is independent of θ. As a consequence, the steady-state mean virulence v^* remains invariant with respect to variations in VTE.

6. Discussion

During an epidemic outbreak, pathogen evolution and disease transmission are interdependent. As vaccines are introduced, vaccination behaviour is influenced by disease transmission; in turn, vaccination behaviour affects the spread of the disease. However, most existing mathematical models focus solely on the interplay between pathogen evolution and disease transmission, or between vaccination behaviour and disease transmission. In this study, we formulated a multi-scale model within a game-theoretic framework, set in the context of imperfect vaccines and voluntary vaccination. The model integrated three interacting processes—disease transmission, vaccination strategy formulation and pathogen evolution—with the aim of investigating pathogen evolution and its effect on disease transmission under vaccination.

In the absence of evolution, we first analyzed the threshold dynamics of the SIIp model (4), obtaining the threshold R_0 for disease persistence or extinction. We numerically observed that model (4) exhibits periodic oscillations. In the context of disease persistence ($R_0 > 1$), based on the Price's equation, we derived the evolution equation for the two traits: average virulence of pathogens within the vaccinated and unvaccinated populations. Under specific conditions for the trade-off function, we examined the positivity and boundedness of the trait equation. Within this framework, we performed numerical simulations to study the long-term impact of pathogen evolution on disease transmission. Specifically, we analyzed the effect of evolutionary speed on the amplitude of the periodic oscillations in the coupled systems (4) and (7), as well as the influence of vaccine efficacy on the epidemic steady state. Next, we further analyzed the scenario limited to the vaccination period, focusing on potential immunity-adapted variants. We categorized the variants into four types and quantitatively described the evolutionary direction of strain types. Additionally, we parameterized the proposed model using the COVID-19 case data in Tokyo, Japan, for illustration. Finally, we considered the case where there was no difference between the vaccinated and unvaccinated populations, reducing the system to the classical vaccination model, and analyzed the dynamical behaviour of this degenerate evolutionary-coupling model.

Our findings demonstrated that co-evolutionary dynamics are highly sensitive to the speed of evolutionary adaptation. As the evolutionary adaptation rates in the two groups increased simultaneously, we observed several distinct phases: population cycling, trait-population cycling, cryptic Red Queen dynamics and stationary phases with rapid adaptation. An intriguing finding of this study is the asymmetric relationship between population dynamics and evolutionary dynamics. Specifically, when the adaptation is fast, microevolutionary changes (like trait adaptation) can occur with larger fluctuations, but macroevolutionary outcomes (such as population size) may be more constrained or buffered, highlighting the complex interplay between individual adaptations and population-level dynamics. However, if two antagonistic traits are considered, such as predator offense versus prey defense, evolution may drive both traits to escalate continuously, resembling an evolutionary arms race. This represents a destabilizing evolutionary feedback, under which both population and trait oscillations may amplify at intermediate evolutionary rates, leading to a resonance-like phenomenon [38,40].

We hypothesize that the vaccine mainly functions in terms of transmissibility. Our results show that the model incorporating both aspiration-based and imitation-based updating rules reflects the autonomous decision-making behaviour of the population. Compared to the simplified model based solely on imitation updating rules, it provides a more realistic description of decision-making dynamics. Based on COVID-19 case data from Tokyo, we observed that if the strain undergoes further adaptation in response to immune priming, our findings indicated that enhancing vaccine uptake is effective in limiting the emergence of detrimental variants. Additionally, the long-term evolutionary outcome may favour the emergence of specialist variants. Furthermore, at this early stage, the limited information drives individuals to rely on the decisions of others, amplifying imitation-based decision-making. Subsequent sensitivity analysis confirmed this interpretation. The dynamics of the simplified model are relatively straightforward, with no stable limit cycles bifurcating from the positive equilibrium. Moreover, the threshold for disease extinction or persistence is fundamentally characterized by a single value.

While previous studies [9,10] used mathematical models to investigate the impact of vaccination on pathogen evolution and disease transmission, our study provides key methodological advances. Firstly, unlike studies that assumed static vaccination strategies [9,10], we treated vaccine uptake as a time-dependent variable and developed a dynamic vaccination strategy model within a game-theoretic framework, integrating both aspiration-based and imitation-based updating rules. The model was calibrated with empirical data, providing a more realistic depiction of decision-making dynamics. Secondly, Day et al. [10] only numerically examined the impact of vaccination on pathogen evolution; however, they did not address the mathematical challenges of ensuring positivity and boundedness in the two-trait system. We overcame these challenges and rigorously analyzed the dynamics of the corresponding degenerate coupled system, comparing it with the fully coupled model. Together, these contributions establish a framework coupling the processes of disease transmission, vaccination strategy formulation and pathogen evolution that constitutes the main advance of our study: a rigorous, multi-scale framework that not only generates novel predictions unattainable under the static strategy assumption but also provides a theoretical foundation for understanding pathogen evolution.

Our study has several limitations, which should be acknowledged. First, the model does not account for the co-evolutionary dynamics between the host and pathogen, which may lead to an overestimation [12] or underestimation [38] of pathogen virulence and disease prevalence, as host–pathogen interactions are inherently antagonistic; future work could consider this process. Second, we have neglected the possibility of vaccine resistance emerging, which could affect vaccination strategy-making in the long term and, in turn, influence the evolutionary trajectory of pathogen virulence. Third, the present model is based on a well-mixed population assumption and does not explicitly account for network structures. Given that physical contact and information networks may substantially shape both epidemic transmission and vaccination decision-making [41], extending the proposed framework to network-structured populations represents an important direction for future research. Fourth, the present framework does not incorporate optimal-control strategies. Recent work has shown that optimal-control theory can be integrated with vaccination game

dynamics to assess socially optimal vaccination policies [42]. Extending the proposed framework to an optimal-control setting would therefore be a promising direction for future research.

In summary, this study innovatively integrated dynamic vaccination strategies into an evolutionary epidemiological model, developing a rigorous multiscale framework that couples the processes of disease transmission, vaccination strategy formulation and pathogen evolution. The coupling is not unidirectional; rather, the three processes mutually influence one another. This work provides key methodological advances for multi-scale mathematical modelling in the context of pathogen evolution and may help to develop a vaccination treatment protocol that is beneficial to the whole population.

CRediT authorship contribution statement

Qiutong Liu: Writing – original draft, Visualization, Software, Methodology, Investigation, Formal analysis; **Stacey R. Smith?:** Writing – review & editing, Validation, Funding acquisition; **Yanni Xiao:** Writing – review & editing, Validation, Supervision, Resources, Project administration, Funding acquisition, Conceptualization.

Declaration of competing interest

The authors declare that they have no competing financial interests or personal relationships that could have appeared to influence the work reported in this paper.

Acknowledgment

This work was funded by the National Natural Science Foundation of China (No. 12220101001 (YXiao)) and by an NSERC Discovery Grant (Smith?). For citation purposes, please note that the question mark in "Smith?" is part of her name.

Data availability

No data was used for the research described in the article.

Appendix A. Rationale for the closure approximation

The behavioural variable $p(t)$ describes vaccine uptake among individuals newly entering the susceptible population. Since the natural birth and death rates are both assumed to be μ, in the absence of infection, the only epidemiological processes affecting the susceptible classes are recruitment and natural mortality. Therefore, at the population level, the susceptible composition is primarily determined by the vaccination uptake $p(t)$, which gives $S_v(t) \approx p(t)S(t)$ and $S_n(t) \approx (1 - p(t))S(t)$. When infection is present, vaccinated and non-vaccinated susceptible individuals experience different infection risks and disease-induced mortality. Nevertheless, $S_v(t)$ remains approximately proportional to $p(t)S(t)$, and $S_n(t)$ remains approximately proportional to $(1 - p(t))S(t)$. Since $p(t)$ acts on the inflow into the susceptible population at the population level, the infected classes usually constitute a relatively small fraction of the total population. Hence, the differential depletion of S_n and S_v caused by infection can be regarded as a relatively small correction to the susceptible composition primarily determined by vaccine uptake among newly susceptible individuals. This provides a reasonable justification for the population-level closure approximation.

To further support this approximation, we compare the numerical solutions of the full five-dimensional system (3) with those of the reduced four-dimensional system (4). As illustrated in Fig. A.1(a)–(c), the solution trajectories of the two systems are very close under the parameter regimes considered, in which $\mu = 0.000001$ is sufficiently small. When periodic oscillations occur, the two models may exhibit some differences in oscillation amplitude. However, these differences do not change the qualitative dynamical behaviour. As shown in Fig. A.1(d), the full system (3) produces results qualitatively consistent with those obtained from the reduced system. Therefore, this approximation does not affect the main conclusions of this study.

We emphasize that the reduced system is not intended to be exactly identical to the full system. Explicitly retaining S_n and S_v would provide a more detailed description of the susceptible population. Nevertheless, the reduced model preserves the key mechanisms relevant to this study: namely, the coupling between vaccination behaviour, infections in vaccinated and non-vaccinated hosts, and pathogen evolution, while simplifying the mathematical analysis. Therefore, this model reduction is meaningful and appropriate for the objectives of the present study.

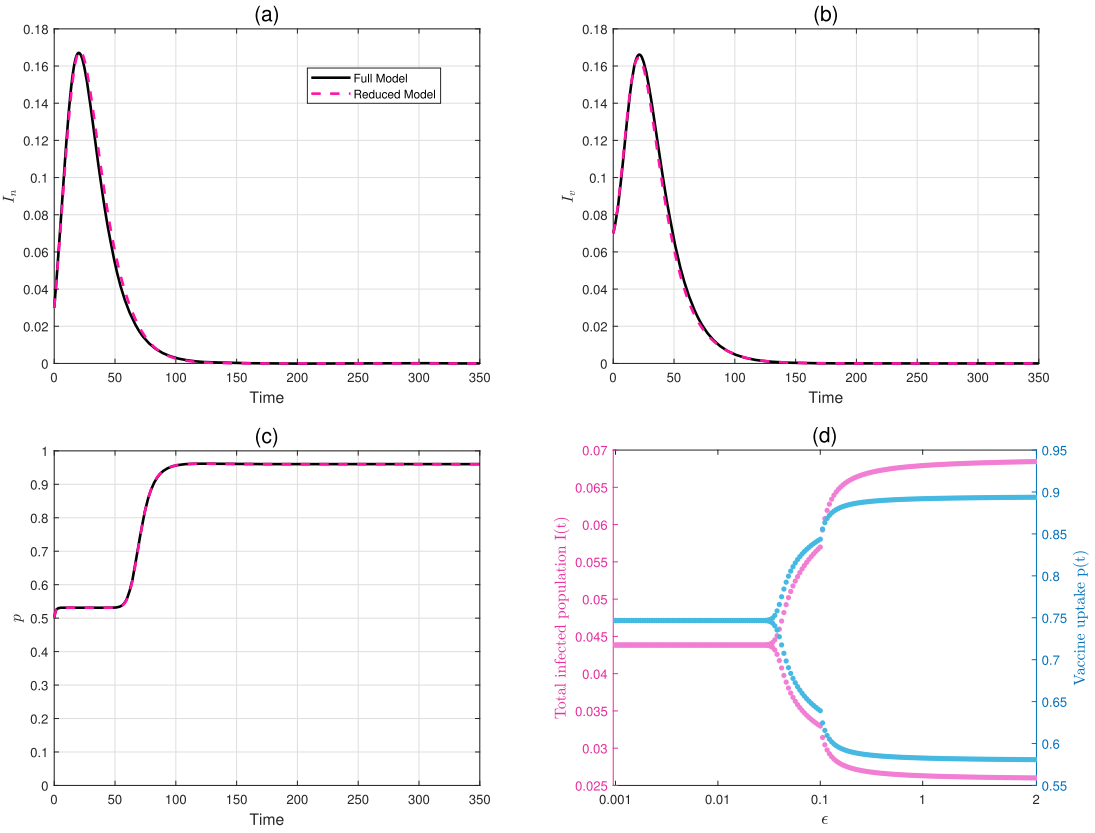

Fig. A.1. (a)–(c) Time series of the reduced system (4) (pink dashed lines) and the full system (3) (black solid lines). The parameter values are $\mu = 0.000001$ and $\beta_{nn} = 0.25$. (d) Bifurcation diagram of the total infected population $I(t)$ and vaccine uptake $p(t)$ with respect to ϵ for system (3), with $\mu = 0.005$ and $\beta_{nn} = 0.85$. The remaining parameter values are $\beta_{vn} = 0.2075$, $\beta_{vv} = 0.119$, $\beta_{nv} = 0.238$, $\alpha_n = 0.02$, $\alpha_v = 0.015$, $\gamma_n = 0.05$, $\gamma_v = 0.05$, $\xi = 0.2$, $h = 80$, $k = 0.001$, $c_n = 2$, $c_v = 1$, $\omega_n = 0.001$, $\omega_v = 0.05$ and $\epsilon = 0.5$. The initial values for the reduced system (4) are $(S(0), I_n(0), I_v(0), p(0))$, while those for the full system (3) are $((1-p(0))S(0), p(0)S(0), I_n(0), I_v(0), p(0))$, where $S(0) = 0.9$, $I_n(0) = 0.03$, $I_v(0) = 0.07$ and $p(0) = 0.5$.

Appendix B. Proof of Theorem 1

By direct calculation, we obtain that the expression of the possible DFE is $E_0 = (1, 0, 0, \bar{p}_0)$, where $\bar{p}_0$ satisfies $\tilde{A}_1\bar{p}_0^2 + \tilde{A}_2\bar{p}_0 + \tilde{A}_3 = 0$, with

$$\tilde{A}_1 = -\epsilon\xi\frac{1-e^{hk}}{1+e^{hk}} > 0,\ \tilde{A}_2 = \epsilon\xi\frac{1-e^{hk}}{1+e^{hk}} - \frac{\epsilon(1-\xi)}{1+e^{h\omega_n}} - \frac{\epsilon(1-\xi)}{1+e^{h(\omega_v-k)}} < 0,\ \tilde{A}_3 = \frac{\epsilon(1-\xi)}{1+e^{h\omega_n}} > 0.$$

Denoting $F(p) = \tilde{A}_1p^2 + \tilde{A}_2p + \tilde{A}_3$, we have

$$F(0) = \tilde{A}_3 > 0,\ F(1) = -\frac{\epsilon(1-\xi)}{1+e^{h(\omega_v-k)}} < 0,\ \triangle = (\tilde{A}_2)^2 - 4\tilde{A}_1\tilde{A}_3 > 0.$$

According to the properties of a quadratic function, there is a unique root $\bar{p}_0 = (-\tilde{A}_2 - \sqrt{\triangle})/(2\tilde{A}_1) \in (0,1)$ such that $F(\bar{p}_0) = 0$. By calculating the spectral radius of the next-generation matrix for model (4), the basic reproduction number R_0 is

$$R_0 = \frac{\beta_{nn}(1-\bar{p}_0)}{\alpha_n+\gamma_n+\mu} + \frac{\beta_{vv}\bar{p}_0}{\alpha_v+\gamma_v+\mu}.$$

Next, we analyse the stability of E_0. The Jacobian matrix of system (4) evaluated at E_0 gives the characteristic equation

$$(\lambda+\mu)(\lambda+\sqrt{\triangle})(\lambda^2+\tilde{B}_1\lambda+\tilde{B}_2) = 0,$$

where

$$\tilde{B}_1 = -\beta_{vv}\bar{p}_0 + \alpha_v+\gamma_v+\mu-\beta_{nn}(1-\bar{p}_0)+\alpha_n+\gamma_n+\mu,$$
$$\tilde{B}_2 = (\alpha_n+\gamma_n+\mu)(\alpha_v+\gamma_v+\mu)(1-R_0).$$

This implies that E_0 is locally asymptotically stable if $R_0 < 1$ and unstable if $R_0 > 1$.

Appendix C. The proof of uniform persistence

Define the set

$$X = \{(S, I_n, I_v, p) : S \geq 0, I_n \geq 0, I_v \geq 0, p \geq 0\},$$
$$X_0 = \{(S, I_n, I_v, p) : S \geq 0, I_n > 0, I_v > 0, p \geq 0\},$$

and

$$\partial X_0 = X \backslash X_0.$$

Then both X and X_0 are positively invariant, and ∂X_0 is relatively closed in X. To prove that the disease is uniformly persistent, it suffices to show that ∂X_0 uniformly repels the solutions of system (4) in X_0. Note that system (4) is point dissipative, since the attracting domain D is a positive invariant set. Define

$$M_\partial = \{(S(t), I_n(t), I_v(t), p(t)) \in \partial X_0 : S(t), I_n(t), I_v(t), p(t) \text{ satisfy system (4)}\}.$$

It suffices to show that $M_\partial = \{(S(t), 0, 0, p(t)) : S(t), p(t) > 0\}$. Suppose not. Then there exists $\varphi_0 = (S(0), I_n(0), I_v(0), p(0)) \in M_\partial$ and $t_0 \geq 0$, such that at least one of the terms in $I_n(t)$ and $I_v(t)$ is greater than 0 at $t = t_0$. If $I_n(t_0) > 0$ and $I_v(t_0) = 0$, then $I_v'(t_0) = \beta_{nv} I_n p S > 0$. That is, $\exists t_1 > 0$ such that $I_n(t) > 0$ and $I_v(t) > 0$ for all $t \in (t_0, t_0 + t_1)$. Hence $(S(t), I_n(t), I_v(t), p(t)) \notin \partial X_0$, which contradicts $\varphi_0 \in M_\partial$. Similarly, we can prove the case $I_n(t_0) = 0$ and $I_v(t_0) > 0$. Thus, we claim $M_\partial = \{(S(t), 0, 0, p(t)) : S(t), p(t) > 0\}$. Clearly, E_0 is the unique fixed point in M_∂. Then if φ_0 is a solution of system (4) initiating from M_∂, we have $U_{\varphi_0 \in M_\partial} = \{E_0\}$. Thus E_0 is the compact isolated invariant set of M_∂ over the initial value φ_0.

In the following, we show that there exists a constant $\eta \in (0, 1)$ when $R_0 > 1$, such that for any solution $u(t, x_0)$, $x_0 \in X_0$, $\limsup_{t \to \infty} ||u(t, x_0) - E_0|| \geq \eta$ is satisfied; that is, $W^S(E_0) \cap X_0 = \emptyset$, where $W^S(E_0)$ is the stable manifold of E_0. We prove it by contradiction. Suppose that $\limsup_{t \to \infty} ||u(t, x_0) - E_0|| < \eta$ for any sufficiently small $\eta > 0$; i.e., there exists a positive constant $t_2 > 0$, for all $t \geq t_2$, such that

$$1 - \eta \leq S(t) \leq 1 + \eta, \quad \bar{p}_0 - \eta \leq p(t) \leq \bar{p}_0 + \eta.$$

Hence, for all $t \geq t_2$, we have

$$\frac{dI_n}{dt} \geq (1 - \eta)(1 - \bar{p}_0 - \eta)(\beta_{nn} I_n + \beta_{vn} I_v) - (\alpha_n + \gamma_n + \mu) I_n,$$
$$\frac{dI_v}{dt} \geq (1 - \eta)(\bar{p}_0 - \eta)(\beta_{nv} I_n + \beta_{vv} I_v) - (\alpha_v + \gamma_v + \mu) I_v.$$

Then when $t \geq t_2$, consider the auxiliary system

$$\frac{dY}{dt} = A_\eta Y, \tag{C.1}$$

where $Y = (I_n, I_v)^T$, and

$$A_\eta = \begin{pmatrix} (1 - \eta)(1 - \bar{p}_0 - \eta)\beta_{nn} - (\alpha_n + \gamma_n + \mu) & (1 - \eta)(1 - \bar{p}_0 - \eta)\beta_{vn} \\ (1 - \eta)(\bar{p}_0 - \eta)\beta_{nv} & (1 - \eta)(\bar{p}_0 - \eta)\beta_{vv} - (\alpha_v + \gamma_v + \mu) \end{pmatrix}.$$

As $\eta \to 0$, the matrix A_η converges to $A_0 = F - V$, where

$$F = \begin{pmatrix} (1 - \bar{p}_0)\beta_{nn} & (1 - \bar{p}_0)\beta_{vn} \\ \bar{p}_0 \beta_{nv} & \bar{p}_0 \beta_{vv} \end{pmatrix}, \quad V = \begin{pmatrix} \alpha_n + \gamma_n + \mu & 0 \\ 0 & \alpha_v + \gamma_v + \mu \end{pmatrix}.$$

Since $R_0 = \rho(FV^{-1}) > 1$, it follows that $s(A_0) > 0$, where $s(\cdot)$ denotes the spectral bound of a matrix. By the continuity of eigenvalues, there exists sufficiently small $\eta > 0$ such that $s(A_\eta) > 0$. Note that matrix A_η is cooperative and irreducible. Let $\lambda_\eta = s(A_\eta) > 0$ be its principal eigenvalue and let $v \gg 0$ be the corresponding positive eigenvector. Then every positive solution of system (C.1) satisfies $Y(t) \geq C e^{\lambda_\eta (t - t_2)} v$ for some constant $C > 0$. By the comparison principle, we have $(I_n(t), I_v(t))^T \geq Y(t)$ for $t \geq t_2$. Therefore, we obtain $I_n(t) + I_v(t) \to \infty$ when $t \to \infty$, which contradicts system (4) being point dissipative. Thus, E_0 is an isolated invariant set in X, and $W^S(E_0) \cap X_0 = \emptyset$.

In conclusion, each of the forward orbits in M_∂ converges to E_0. Further, E_0 is aperiodic in M_∂. By Theorem 4.3 and Remark 4.3 of [36], we can conclude that ∂X_0 repels uniformly the solutions of (4) in X_0.

Appendix D. Derivation of mean virulence model (7)

We assume that n_p different pathogen strains compete within a heterogeneous host population consisting of naïve and vaccinated individuals and that the pathogen population may be polymorphic at any given time. For the sake of simplicity, multiple infections are not allowed. We first extend model (4) to multiple strains and focus only on infectious compartments, which gives

$$\frac{dI_n^i}{dt} = r_{nn}(i) I_n^i + r_{vn}(i) I_v^i,$$
$$\frac{dI_v^i}{dt} = r_{vv}(i) I_v^i + r_{nv}(i) I_n^i,$$

where

$$r_{nn}(i)=\beta^i_{nn}(1-p)S-\alpha^i_n-\gamma_n-\mu,\quad r_{vn}(i)=\beta^i_{vn}(1-p)S,$$
$$r_{vv}(i)=\beta^i_{vv}pS-\alpha^i_v-\gamma_v-\mu,\quad r_{nv}(i)=\beta^i_{nv}pS.$$

Here, i is the strain index, which varies between 1 and n_p. In each generation, mutation selection within different host types and migration between host types jointly affect the evolution of mean virulence levels. Following [18] (Eqs. (2.9)–(2.10)), the evolutionary dynamics of mean virulence level can be derived as

$$\frac{d\bar V_n}{dt}=\underset{n}{\mathrm{cov}}(V,r_{nn})-\mu(\bar V_n-\bar V^m_n)+\frac{I_v}{I_n}\underset{v}{\mathrm{cov}}(V,r_{vn})+\frac{I_v}{I_n}\bar r_{vn}(\bar V_v-\bar V_n),$$
$$\frac{d\bar V_v}{dt}=\underset{v}{\mathrm{cov}}(V,r_{vv})-\mu(\bar V_v-\bar V^m_v)+\frac{I_n}{I_v}\underset{n}{\mathrm{cov}}(V,r_{nv})+\frac{I_n}{I_v}\bar r_{nv}(\bar V_n-\bar V_v),$$

where μ is the mutation rate for all strains, $\bar V^m_j$ is the average trait of all of mutations that arise in j type hosts and $\bar r_{jz}$ is calculated over the distribution $q^i_j=I^i_j/I_j$ $(j,z\in\{n,v\})$. The covariance between a and b across all strains among j type hosts is $\underset{j}{\mathrm{cov}}(a,b)$. Assume that the distribution of V_j in the population is concentrated around the population mean $\bar V_j$ $(j\in\{n,v\})$. Using a Taylor expansion around $V_j=\bar V_j$, we can approximate the function r_{jz} $(j,z\in\{n,v\})$ by picking up leading terms only [10]. This yields

$$\begin{aligned}\frac{d\bar V_n}{dt}&\approx\underset{n}{\mathrm{var}}(V)r'_{nn}(V_n)\mid_{V_n=\bar V_n}-\mu(\bar V_n-\bar V^m_n)+\frac{I_v}{I_n}\underset{v}{\mathrm{var}}(V)r'_{vn}(V_v)\mid_{V_v=\bar V_v}+\frac{I_v}{I_n}\bar r_{vn}(\bar V_v-\bar V_n),\\ \frac{d\bar V_v}{dt}&\approx\underset{v}{\mathrm{var}}(V)r'_{vv}(V_v)\mid_{V_v=\bar V_v}-\mu(\bar V_v-\bar V^m_v)+\frac{I_n}{I_v}\underset{n}{\mathrm{var}}(V)r'_{nv}(V_n)\mid_{V_n=\bar V_n}+\frac{I_n}{I_v}\bar r_{nv}(\bar V_n-\bar V_v),\end{aligned}\tag{D.1}$$

where $\underset{n}{\mathrm{var}}(V)$ and $\underset{v}{\mathrm{var}}(V)$ are the phenotypic variances in strain types among naïve and vaccinated hosts, respectively. Denote $G_n=\underset{n}{\mathrm{var}}(V)/t_g$ and $G_v=\underset{v}{\mathrm{var}}(V)/t_g$, where t_g is the generation time of the parasite strains. G_n and G_v represent the corresponding evolutionary adaptation rates [38]. Without loss of generality, we assume $t_g=1$; i.e., the generation time of parasite strains coincides with a unit time scale of the population dynamics [11,38]. Applying Eq. (D.1) under the assumption of negligible mutation yields Eq. (7) in the main text.

Appendix E. The positivity and boundedness of trait dynamics (7)

Since

$$\left.\frac{d\bar V_n}{dt}\right|_{\bar V_n=0}=G_v\frac{I_v}{I_n}(1-p)S\beta'(\bar V_v)+\frac{I_v}{I_n}(1-p)S\beta(\bar V_v)\bar V_v\ge 0,$$
$$\left.\frac{d\bar V_v}{dt}\right|_{\bar V_v=0}=G_n\frac{I_n}{I_v}\theta pS\beta'(\bar V_n)+\frac{I_n}{I_v}\theta pS\beta(\bar V_n)\bar V_n\ge 0,$$

it follows that $\bar V_j(t)\ge 0$ for all $t>0$ whenever $\bar V_j(0)\ge 0$ $(j\in\{n,v\})$. The transmission function $\beta_j(V_j)$ is assumed to be a saturated response [43]. Here, saturation means that $\beta_j(V_j)$ remains bounded for $V_j\in\mathbb{R}_+$ and approaches a finite limiting value as $V_j\to\infty$. On the assumption that we adopt the trade-off forms in (8), direct calculation yields $\beta(V_j)\le\frac{\beta_0}{h_v}$ and $\beta'(V_j)\le\frac{9\beta_0}{8\sqrt{3h_v}}<\frac{\beta_0}{\sqrt{h_v}}$. Since $S,p\le 1$, we have

$$\frac{d\bar V_n}{dt}\le G_n\frac{\beta_0}{\sqrt{h_v}}+G_v\frac{I_v}{I_n}\frac{\beta_0}{\sqrt{h_v}}-2G_n\alpha_0\bar V_n+\frac{I_v}{I_n}\frac{\beta_0}{h_v}max\{\bar V_v-\bar V_n,0\},$$
$$\frac{d\bar V_v}{dt}\le G_v\frac{\beta_0}{\sqrt{h_v}}+G_n\frac{I_n}{I_v}\frac{\beta_0}{\sqrt{h_v}}-2G_v\alpha_0\bar V_v+\frac{I_n}{I_v}\frac{\beta_0}{h_v}max\{\bar V_n-\bar V_v,0\}.$$

Denoting $y=I_n/I_v$, we have

$$\begin{aligned}\frac{dy}{dt}&=(\beta_{nn}y+\beta_{vn})(1-p)S-\alpha_n y-\gamma_n y-\mu y-y((\beta_{vv}+\beta_{nv}y)pS-\alpha_v-\gamma_v-\mu)\\&\le\beta_{vn}+(\beta_{nn}-\alpha_n-\gamma_n-\mu-\beta_{vv}pS+\alpha_v+\gamma_v+\mu)y-\beta_{nv}pSy^2\\&=A+By-Cy^2.\end{aligned}$$

Note that $S(t)>0$ and $p(t)>0$ for all $t>0$ provided that $S(0)>0$ and $p(0)>0$. It then follows from the comparison principle that $y(t)\le\max\{y(0),\frac{B+\sqrt{B^2+4AC}}{2C}\}$. Likewise, we have similar conclusions about I_v/I_n. That is, there exist positive constants M_1 and M_2 such that $I_v/I_n<M_1$ and $I_n/I_v<M_2$ for all $t>0$. Then we obtain

$$\begin{aligned}\frac{d\bar V_n}{dt}&\le G_n\frac{\beta_0}{\sqrt{h_v}}+G_vM_1\frac{\beta_0}{\sqrt{h_v}}-2G_n\alpha_0\bar V_n+M_1\frac{\beta_0}{h_v}\max\{\bar V_v-\bar V_n,0\},\\ \frac{d\bar V_v}{dt}&\le G_v\frac{\beta_0}{\sqrt{h_v}}+G_nM_2\frac{\beta_0}{\sqrt{h_v}}-2G_v\alpha_0\bar V_v+M_2\frac{\beta_0}{h_v}\max\{\bar V_n-\bar V_v,0\}.\end{aligned}\tag{E.1}$$

Denote $A_n = G_n\frac{\beta_0}{\sqrt{h_v}} + G_v M_1\frac{\beta_0}{\sqrt{h_v}}$ and $A_v = G_v\frac{\beta_0}{\sqrt{h_v}} + G_n M_2\frac{\beta_0}{\sqrt{h_v}}$. Further, we discuss inequality system (E.1) separately in the following three regions: (I) $\bar{V}_n > \bar{V}_v$; (II) $\bar{V}_n < \bar{V}_v$; (III) $\bar{V}_n = \bar{V}_v$. For region (I), we have

$$\frac{d\bar{V}_n}{dt} \le A_n - 2G_n\alpha_0\bar{V}_n,$$
$$\frac{d\bar{V}_v}{dt} \le A_v - 2G_v\alpha_0\bar{V}_v + M_2\frac{\beta_0}{h_v}(\bar{V}_n - \bar{V}_v).$$

By the comparison principle, we obtain $\bar{V}_n(t) \le \max\{\bar{V}_n(0), \frac{A_n}{2G_n\alpha_0}\}$. Then we have

$$\frac{d\bar{V}_v}{dt} \le A_v + M_2\frac{\beta_0}{h_v}\max\left\{\bar{V}_n(0), \frac{A_n}{2G_n\alpha_0}\right\} - \left(2G_v\alpha_0 + M_2\frac{\beta_0}{h_v}\right)\bar{V}_v.$$

Hence, we derive

$$\bar{V}_v \le \max\left\{\bar{V}_v(0), \frac{A_v + M_2\frac{\beta_0}{h_v}\max\left\{\bar{V}_n(0), \frac{A_n}{2G_n\alpha_0}\right\}}{2G_v\alpha_0 + M_2\frac{\beta_0}{h_v}}\right\} \equiv A_1.$$

Likewise, for region (II), we could obtain a conclusion analogous to that of region (I). That is, there exists a constant A_2, such that $\bar{V}_n \le A_2$. For region (III), we have $\frac{d\bar{V}_j}{dt} \le A_j - 2G_j\alpha_0\bar{V}_j$, $j \in \{n, v\}$. It follows from the comparison principle that $\bar{V}_j(t) \le \max\{\bar{V}_j(0), \frac{A_j}{2G_j\alpha_0}\}$.

Define $H = 2\max\left\{\frac{A_n}{2G_n\alpha_0}, \frac{A_v}{2G_v\alpha_0}, A_1, A_2, \bar{V}_n(0), \bar{V}_v(0)\right\}$. Next, we show that $R_{ec} \equiv [0, H]\times[0, H]$ is a positively invariant rectangle of the trait model (7). We need to verify that when $(\bar{V}_n, \bar{V}_v)$ is on the boundary of the rectangle R_{ec}, the vector field of the system points inward toward the interior of the rectangle or along the boundary. When $\bar{V}_n = H$ and $\bar{V}_v \in [0, H]$, direct calculation yields

$$\left.\frac{d\bar{V}_n}{dt}\right|_{\bar{V}_n=H} \le A_n - 2G_n\alpha_0 H < 0.$$

Similarly, when $\bar{V}_v = H$ and $\bar{V}_n \in [0, H]$, direct calculation yields

$$\left.\frac{d\bar{V}_v}{dt}\right|_{\bar{V}_v=H} \le A_v - 2G_v\alpha_0 H < 0.$$

Appendix F. Bifurcation diagrams in different planes related to G.

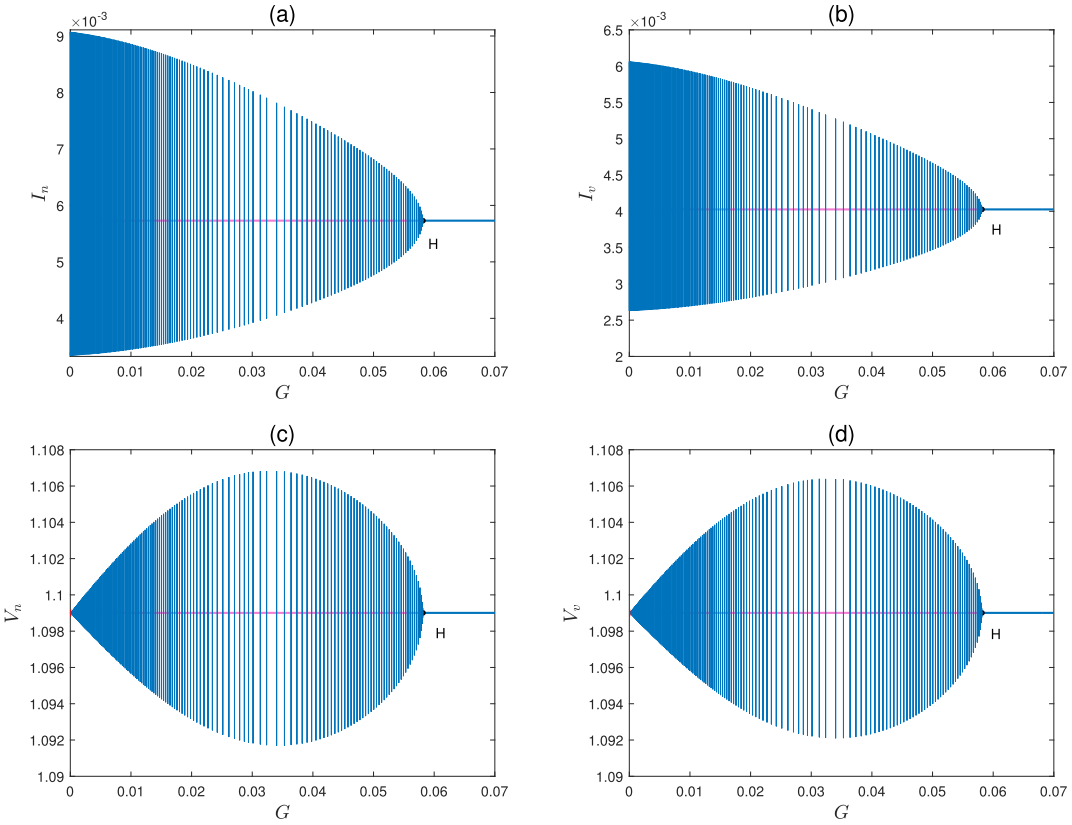

Fig. F.1. Bifurcation diagrams in different planes related to G. The blue curves represent stable equilibria, the pink curves represent unstable equilibria, and a black dot marked with "H" (when $G = 0.0583$) indicates that the coupled evolutionary system undergoes a Hopf bifurcation. The first Lyapunov coefficient at the Hopf point is negative, indicating that the Hopf bifurcation is supercritical and the resulting periodic orbit is stable. Parameters are as in Fig. 3.

Appendix G. Effects of differing evolutionary adaptation rates ($G_n \neq G_v$) on oscillation amplitude

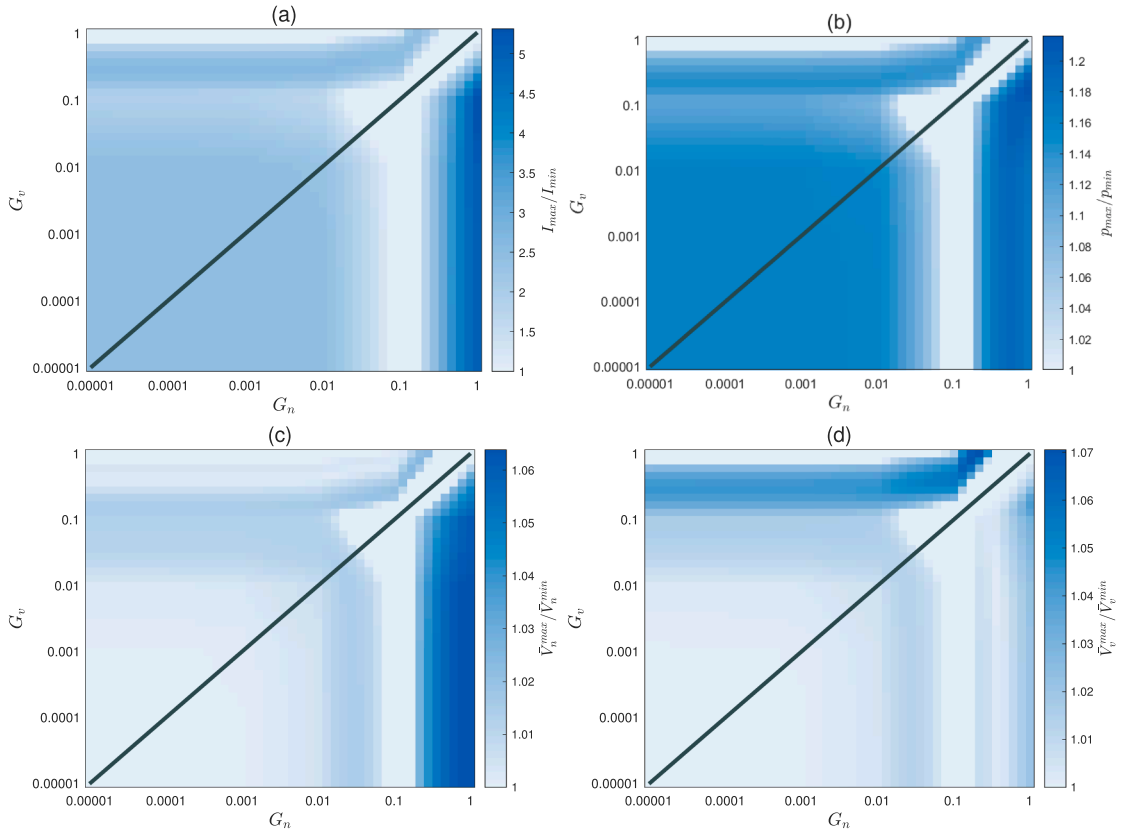

Fig. G.1. Effects of differing evolutionary adaptation rates ($G_n \neq G_v$) on the oscillation amplitude level. The grey diagonal line represents $G_n = G_v$ (corresponding to the result shown in Fig. 3). Parameters are as in Fig. 3.

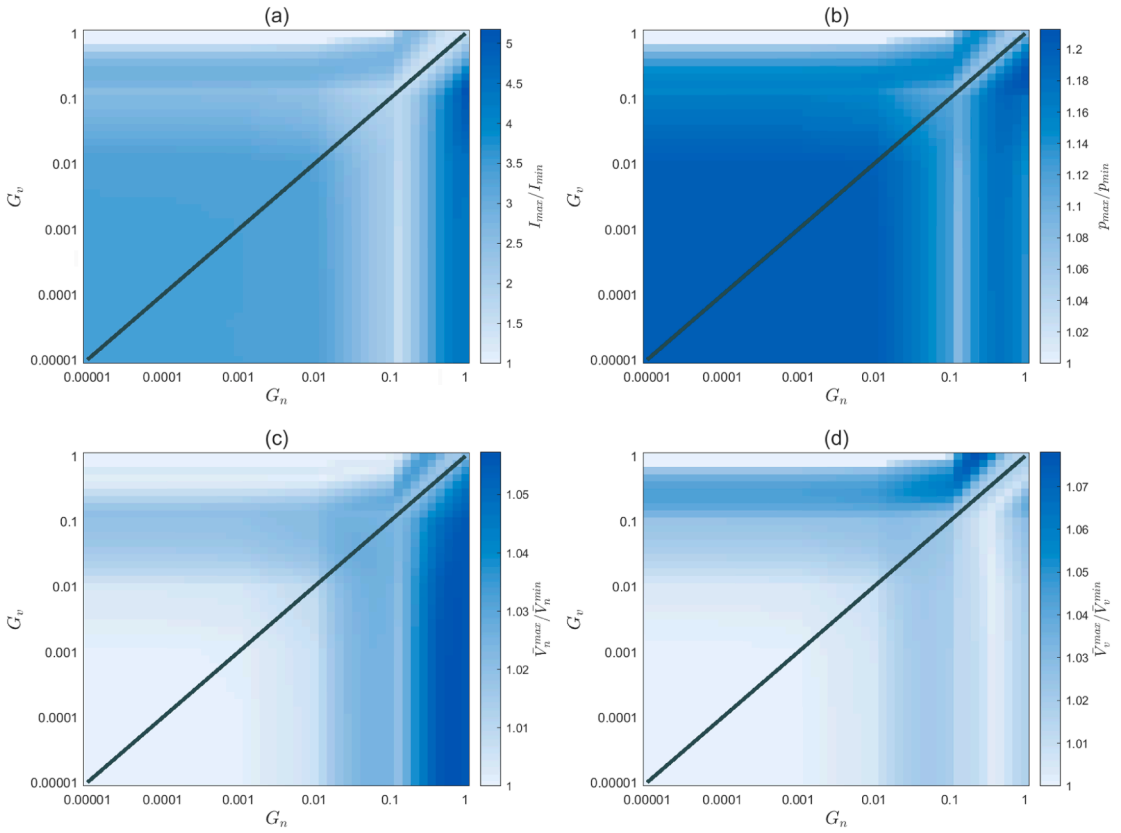

Fig. G.2. Effects of differing evolutionary adaptation rates ($G_n \neq G_v$) on the oscillation amplitude level. The grey diagonal line represents $G_n = G_v$ (corresponding to the result shown in Fig. 4). Parameters are as in Fig. 4.

Appendix H. Derivation of the fitness f^i and selection coefficient s of variant i

In the following, we derive the absolute growth rate f^i and the corresponding selection coefficient s for variant i based on the epidemic model (4). We track the dynamics of variant i using the following system of differential equations:

$$\frac{dI_n^i}{dt} = (1-p)S(\beta_{nn}^i I_n^i + \beta_{vn}^i I_v^i) - \alpha_n^i I_n^i - \gamma_n^i I_n^i - \mu I_n^i,$$
$$\frac{dI_v^i}{dt} = pS(\beta_{nv}^i I_n^i + \beta_{vv}^i I_v^i) - \alpha_v^i I_v^i - \gamma_v^i I_v^i - \mu I_v^i.$$

The reproductive success of variant i depends on three fitness components: transmission rates (β^i), disease-induced mortalities (α^i) and infectious periods ($1/\gamma^i$) in naïve and vaccinated hosts, respectively. The per capita growth rate of infections is governed by the dominant eigenvalue f^i of the corresponding transmission matrix R_i [9,44]""

$$R_i = \begin{pmatrix} (1-p)S\beta_{nn}^i - \alpha_n^i - \gamma_n^i - \mu & (1-p)S\beta_{vn}^i \\ pS\beta_{nv}^i & pS\beta_{vv}^i - \alpha_v^i - \gamma_v^i - \mu \end{pmatrix}.$$

Here, the density of susceptible hosts S is regarded as a slow variable relative to the infection dynamics of variant i [9]. Define $\delta_\alpha^i = \alpha_v^i - \alpha_n^i$ and $\delta_\gamma^i = \gamma_v^i - \gamma_n^i$. Then we have

$$f^i = (1-p)f_n^i + pf_v^i - \frac{pS\beta_{vv}^i}{(1-p)S\beta_{nn}^i + pS\beta_{vv}^i}(\delta_\alpha^i + \delta_\gamma^i) + o\left(\sqrt{(\delta_\alpha^i)^2 + (\delta_\gamma^i)^2}\right),$$

with

$$f_n^i = \beta_{nn}^i S - \alpha_n^i - \gamma_n^i - \mu, \quad f_v^i = \beta_{vv}^i S - \alpha_v^i - \gamma_v^i - \mu,$$

where f_n^i and f_v^i are the fitnesses of variant i in fully naïve and vaccinated hosts, respectively. Assuming that the disease-induced mortality rate and the recovery rate among hosts differ only slightly ($\alpha_n^i \approx \alpha_v^i$ and $\gamma_n^i \approx \gamma_v^i$), the fitness f^i can be simplified as

$$f^i = (1-p)f_n^i + pf_v^i.$$

In what follows, we consider the selection coefficient s. For simplicity, we assume that the effects of mutation on the different viral fitness components within the host j are small and denote them as

$$\Delta\beta_{jj} = \beta_{jj}^m - \beta_{jj}^w, \quad \Delta\alpha_j = \alpha_j^m - \alpha_j^w, \quad \Delta\gamma_j = \gamma_j^m - \gamma_j^w,$$

where β_{jj}^w, α_j^w and γ_j^w (resp., β_{jj}^m, α_j^m and γ_j^m) are the fitness components of the wild type (resp., mutant) and $j \in \{n, v\}$. Accordingly, the fitness (growth rate) of the wild-type population is given by

$$f^w = (1-p)f_n^w + pf_v^w,$$

and the fitness of the novel variant is $f^m = (1-p)f_n^m + pf_v^m = f^w + s$, where

$$s = (1-p)\Delta f_n + p\Delta f_v,$$

with

$$\Delta f_n = f_n^m - f_n^w = S\Delta\beta_{nn} - \Delta\alpha_n - \Delta\gamma_n, \quad \Delta f_v = f_v^m - f_v^w = S\Delta\beta_{vv} - \Delta\alpha_v - \Delta\gamma_v.$$

That is, Δf_n and Δf_v are the differences in fitness between the variant and the wild type in fully naïve and fully vaccinated populations, respectively.

Appendix I. Proof of Theorem 5

By simple calculation, the Jacobian matrix at E_{01}^n has three negative eigenvalues: $-\mu$, $-\gamma-\mu$, $-k\epsilon\rho$, and the other eigenvalue is $2G(\beta_0-\alpha_0)$. The Jacobian matrix at E_{02}^n has three negative eigenvalues: $-\mu$, $-k\epsilon\rho$, $G(\beta''(v_0^n)-\alpha''(v_0^n))$, and the other eigenvalue is $\beta(v_0^n)-\alpha(v_0^n)-\gamma-\mu$. The Jacobian matrix at E_{01}^v and E_{02}^v both have a positive eigenvalue $k\epsilon\rho$. This implies that the equilibrium E_{01}^n is locally asymptotically stable if $\beta_0 < \alpha_0$; when $\beta_0 > \alpha_0$, E_{02}^n is locally asymptotically stable if $R_g^n < 1$, while E_{01}^v and E_{02}^v are always unstable.

Next we examine local stability of the possible endemic equilibria. For $R_c > 1$, the characteristic equation of E_n^* is $\lambda^4 + a_1^n\lambda^3 + a_2^n\lambda^2 + a_3^n\lambda + a_4^n = 0$, where

$$\begin{aligned}
a_1^n &= \beta(v^*)I_n^* + \mu - G(\beta''(v^*)S_n^* - \alpha''(v^*)) - k\epsilon\rho(mI_n^* - 1),\\
a_2^n &= \beta(v^*)^2S_n^*I_n^* - G(\beta''(v^*)S_n^* - \alpha''(v^*))(\beta(v^*)I_n^* + \mu) + G\beta'(v^*)^2S_n^*I_n^*\\
&\quad - k\epsilon\rho(mI_n^* - 1)(\beta(v^*)I_n^* + \mu - G(\beta''(v^*)S_n^* - \alpha''(v^*))),\\
a_3^n &= -G(\beta''(v^*)S_n^* - \alpha''(v^*))\beta(v^*)^2S_n^*I_n^* - k\epsilon\rho(mI_n^* - 1)(\beta(v^*)^2S_n^*I_n^*\\
&\quad - G(\beta''(v^*)S_n^* - \alpha''(v^*))(\beta(v^*)I_n^* + \mu) + G\beta'(v^*)^2S_n^*I_n^*),\\
a_4^n &= k\epsilon\rho(mI_n^* - 1)G(\beta''(v^*)S_n^* - \alpha''(v^*))\beta(v^*)^2S_n^*I_n^*.
\end{aligned}$$

Simple algebraic manipulation yields that $k\epsilon\rho(mI_n^* - 1)$ is an eigenvalue. Assuming $m < m_b$, we derive $k\epsilon\rho(mI_n^* - 1) < 0$. Since $\beta''(v^*)S_n^* - \alpha''(v^*) = -4\alpha_0h_vv^{*2}/(1+h_vv^{*2}) < 0$, it is evident that $a_1^n > 0$, $a_1^na_2^n - a_3^n > 0$ and $a_3^n(a_1^na_2^n - a_3^n) - (a_1^n)^2a_4^n > 0$ hold true when $m < m_b$, where

$$\begin{aligned}
a_1^na_2^n - a_3^n = {}& (\beta(v^*)I_n^* + \mu)[\beta(v^*)^2S_n^*I_n^* - G(\beta''(v^*)S_n^* - \alpha''(v^*))(\beta(v^*)I_n^* + \mu)\\
&+ G\beta'(v^*)^2S_n^*I_n^* - k\epsilon\rho(mI_n^* - 1)(\beta(v^*)I_n^* + \mu - G(\beta''(v^*)S_n^* - \alpha''(v^*)))]\\
&+ G(\beta''(v^*)S_n^* - \alpha''(v^*))[k\epsilon\rho(mI_n^* - 1)(\beta(v^*)I_n^* + \mu - G(\beta''(v^*)S_n^* - \alpha''(v^*)))\\
&+ G(\beta''(v^*)S_n^* - \alpha''(v^*))(\beta(v^*)I_n^* + \mu) - G\beta'(v^*)^2S_n^*I_n^*]\\
&+ k\epsilon\rho(mI_n^* - 1)[k\epsilon\rho(mI_n^* - 1)(\beta(v^*)I_n^* + \mu - G(\beta''(v^*)S_n^* - \alpha''(v^*)))]
\end{aligned}$$

and

$$\begin{aligned}
a_3^n(a_1^na_2^n - a_3^n) - (a_1^n)^2a_4^n = {}& [-\beta(v^*)^2S_n^*I_n^*(G(\beta''(v^*)S_n^* - \alpha''(v^*)) + k\epsilon\rho(mI_n^* - 1))\\
&+ k\epsilon\rho(mI_n^* - 1)G(\beta''(v^*)S_n^* - \alpha''(v^*))(\beta(v^*)I_n^* + \mu)\\
&- k\epsilon\rho(mI_n^* - 1)G\beta'(v^*)^2S_n^*I_n^*][(\beta(v^*)I_n^* + \mu)(-G(\beta''(v^*)S_n^* - \alpha''(v^*))(\beta(v^*)I_n^* + \mu)\\
&+ G\beta'(v^*)^2S_n^*I_n^*) - (\beta(v^*)I_n^* + \mu)^2k\epsilon\rho(mI_n^* - 1)\\
&- G(\beta''(v^*)S_n^* - \alpha''(v^*))(-G(\beta''(v^*)S_n^* - \alpha''(v^*))(\beta(v^*)I_n^* + \mu) + G\beta'(v^*)^2S_n^*I_n^*)\\
&+ k^2\epsilon^2\rho^2(mI_n^* - 1)^2(\beta(v^*)I_n^* + \mu)].
\end{aligned}$$

Combining the Routh–Hurwitz stability criterion, we conclude that E_n^* is locally asymptotically stable if $m < m_b$.

For $\theta R_c > 1$, the characteristic equation of E_v^* is $\lambda^4 + a_1^v\lambda^3 + a_2^v\lambda^2 + a_3^v\lambda + a_4^v = 0$, where

$$\begin{aligned}
a_1^v &= \theta\beta(v^*)I_v^* + \mu - G(\theta\beta''(v^*)S_v^* - \alpha''(v^*)) + k\epsilon\rho(mI_v^* - 1),\\
a_2^v &= \theta^2\beta(v^*)^2S_v^*I_v^* - G(\theta\beta''(v^*)S_v^* - \alpha''(v^*))(\theta\beta(v^*)I_v^* + \mu) + G\theta^2\beta'(v^*)^2S_v^*I_v^*\\
&\quad + k\epsilon\rho(mI_v^* - 1)(\theta\beta(v^*)I_v^* + \mu - G(\theta\beta''(v^*)S_v^* - \alpha''(v^*))),\\
a_3^v &= -G(\theta\beta''(v^*)S_v^* - \alpha''(v^*))\theta^2\beta(v^*)^2S_v^*I_v^* + k\epsilon\rho(mI_v^* - 1)(\theta^2\beta(v^*)^2S_v^*I_v^*\\
&\quad - G(\theta\beta''(v^*)S_v^* - \alpha''(v^*))(\theta\beta(v^*)I_v^* + \mu) + G\theta^2\beta'(v^*)^2S_v^*I_v^*),\\
a_4^v &= -k\epsilon\rho(mI_v^* - 1)G(\theta\beta''(v^*)S_v^* - \alpha''(v^*))\theta^2\beta(v^*)^2S_v^*I_v^*.
\end{aligned}$$

Simple algebraic manipulation yields that $-k\epsilon\rho(mI_v^* - 1)$ is an eigenvalue. Assuming $m > m_t$, we derive $k\epsilon x(mI_v^* - 1) > 0$. Since $\theta\beta''(v^*)S_v^* - \alpha''(v^*) = -4\alpha_0h_vv^{*2}/(1 + h_vv^{*2}) < 0$, direct calculation yields that $a_1^v > 0$, $a_1^va_2^v - a_3^v > 0$ and $a_3^v(a_1^va_2^v - a_3^v) - (a_1^v)^2a_4^v > 0$ hold true when $m > m_t$. Combining the Routh–Hurwitz stability criterion, we conclude that E_v^* is locally asymptotically stable if $m > m_t$.

For $(1 - p^* + \theta p^*)R_c > 1$ and $m \in (m_b, m_t)$, the characteristic equation of E^* is $\lambda^4 + a_1\lambda^3 + a_2\lambda^2 + a_3\lambda + a_4 = 0$, where

$$\begin{aligned}
a_1 &= (1 - p^* + \theta p^*)\beta(v^*)I^* + \mu - G((1 - p^* + \theta p^*)\beta''(v^*)S^* - \alpha''(v^*)),\\
a_2 &= (1 - p^* + \theta p^*)^2\beta(v^*)^2S^*I^* - G((1 - p^* + \theta p^*)\beta''(v^*)S^* - \alpha''(v^*))((1 - p^* + \theta p^*)\beta(v^*)I^* + \mu)\\
&\quad + G(1 - p^* + \theta p^*)^2\beta'(v^*)^2S^*I^* + k\epsilon\rho p^*(1 - p^*)(1 - \theta)\beta(v^*)S^*,\\
a_3 &= -G((1 - p^* + \theta p^*)\beta''(v^*)S^* - \alpha''(v^*))(1 - p^* + \theta p^*)^2\beta(v^*)^2S^*I^*\\
&\quad - k\epsilon\rho p^*(1 - p^*)(1 - \theta)\beta(v^*)S^*(G((1 - p^* + \theta p^*)\beta''(v^*)S^* - \alpha''(v^*)) - \mu),\\
a_4 &= -G((1 - p^* + \theta p^*)\beta''(v^*)S^* - \alpha''(v^*))k\epsilon\rho p^*(1 - p^*)(1 - \theta)\beta(v^*)S^*\mu.
\end{aligned}$$

Since $(1 - p^* + \theta p^*)\beta''(v^*)S^* - \alpha''(v^*) = -4\alpha_0h_vv^{*2}/(1 + h_vv^{*2}) < 0$, direct calculation yields that $a_1 > 0$, $a_1a_2 - a_3 > 0$ and $a_3(a_1a_2 - a_3) - (a_1)^2a_4 > 0$ hold true. Combining the Routh–Hurwitz stability criterion, we conclude that E^* is locally asymptotically stable whenever it exists.

To show the global stability of $E_{01}^n = (1, 0, 0, 0)$, we consider the following Lyapunov function: $V_1(I, \bar{V}) = I(t) + \bar{V}(t)$. The time derivative of $V_1(I, \bar{V})$ computed along solutions of the simplified system (11) is

$$\begin{aligned}
\frac{dV_1}{dt} &= (1 - p + \theta p)\beta(\bar{V})SI - \alpha(\bar{V})I - \gamma I - \mu I + G((1 - p + \theta p)\beta'(\bar{V})S - \alpha'(\bar{V}))\\
&= (1 - p + \theta p)\frac{\beta_0\bar{V}^2}{1 + h_v\bar{V}^2}SI - \alpha_0\bar{V}^2I - \gamma I - \mu I + 2G\bar{V}\left((1 - p + \theta p)\frac{\beta_0S}{(1 + h_v\bar{V}^2)^2} - \alpha_0\right)\\
&\le \beta_0\bar{V}^2I - \alpha_0\bar{V}^2I + 2G\bar{V}(\beta_0 - \alpha_0)\\
&= (\beta_0 - \alpha_0)(\bar{V}I + 2G)\bar{V}.
\end{aligned}$$

As all parameters are positive, if $\beta_0 < \alpha_0$, then $dV_1/dt \le 0$ for all $I(t), \bar{V}(t) \ge 0$ with $dV_1/dt = 0$ only at $I(t) = \bar{V}(t) = 0$. Applying LaSalle's invariant set principle, we have $\lim_{t\to\infty} I(t) = \lim_{t\to\infty} \bar{V}(t) = 0$, which together with (11) imply $\lim_{t\to\infty} S(t) = 1$ and $\lim_{t\to\infty} p(t) = 0$. Hence, E_{01}^n is a global attractor of the simplified system in $\mathcal{D}_s$ when $\beta_0 < \alpha_0$.

To show the global stability of $E_{02}^n = (1, 0, 0, v_0^n)$, we consider the following Lyapunov function: $V_2(I) = I(t)$, which has the following property along the simplified system

$$\begin{aligned}
\frac{dV_2}{dt} &= (1 - p + \theta p)\beta(\bar{V})SI - \alpha(\bar{V})I - \gamma I - \mu I\\
&\le \beta(\bar{V})SI - \alpha(\bar{V})I - \gamma I - \mu I\\
&\le \left(\frac{\beta_0\bar{V}^2}{1 + h_v\bar{V}^2} - \alpha_0\bar{V}^2 - \gamma - \mu\right)I,\\
&= (\alpha_0\bar{V}^2 + \gamma + \mu)\left(\frac{\beta_0\bar{V}^2}{(1 + h_v\bar{V}^2)(\alpha_0\bar{V}^2 + \gamma + \mu)} - 1\right)I.
\end{aligned}$$

Let

$$F(\bar{V}) = \frac{\beta_0\bar{V}^2}{(1 + h_v\bar{V}^2)(\alpha_0\bar{V}^2 + \gamma + \mu)}, \quad H(\bar{V}) = (\alpha_0\bar{V}^2 + \gamma + \mu)(F(\bar{V}) - 1).$$

Simple calculation yields that the equilibrium value v_0^n is the maximum point of $H(\bar{V})$ in $\mathcal{D}_s$. Note that $F(v_0^n) = R_g^n$, so

$$\frac{dV_2}{dt} \le (\alpha_0\bar{V}^2 + \gamma + \mu)(R_g^n - 1)I.$$

Recall that v_0^n exists iff $\beta_0 > \alpha_0$. Since all parameters are positive, if $R_g^n < 1$ and $\beta_0 > \alpha_0$, then $dV_2/dt \le 0$ for all $I(t) \ge 0$ with $dV_2/dt = 0$ only at $I(t) = 0$. Applying LaSalle's invariant set principle, we have $\lim_{t\to\infty} I(t) = 0$, which together with system (11) imply $\lim_{t\to\infty} S(t) = 1$ and $\lim_{t\to\infty} p(t) = 0$. Bring them into the third equation of system (11), we have $d\bar{V}/dt = G(\beta'(\bar{V}) - \alpha'(\bar{V}))$. It is easy to show that

$\lim_{t\to\infty} \bar{V}(t) = v_0^n$ for any $\bar{V}(0) \in \mathbb{R}_+\backslash\{0\}$. Hence, $E_{02}^n(1,0,0,v_0^n)$ is a global attractor of the simplified system in $D_s\backslash\{E_{01}^n\}$ when $\beta_0 > \alpha_0$ and $R_g^n < 1$.

Finally, we investigate the relationship between the thresholds R_g^n and R_c. Simple calculation yields

$$R_c = \frac{\beta(v^*)}{\alpha(v^*)+\gamma+\mu} = \frac{\beta_0}{(\sqrt{\alpha_0}+\sqrt{h_v(\gamma+\mu)})^2},$$

$$R_g^n = \frac{\beta(v_0^n)}{\alpha(v_0^n)+\gamma+\mu} = \frac{\sqrt{\beta_0}(\sqrt{\beta_0}-\sqrt{\alpha_0})}{\sqrt{\alpha_0}(\sqrt{\beta_0}-\sqrt{\alpha_0})+h_v(\mu+\gamma)},$$

indicating that $R_c > 1$ implies $\beta_0 > \alpha_0$. Given $\beta_0 > \alpha_0$, we obtain that

$$R_g^n > 1 \Leftrightarrow (\sqrt{\beta_0}-\sqrt{\alpha_0})^2 > h_v(\mu+\gamma).$$

Note that

$$R_c > 1 \Leftrightarrow \beta_0 > (\sqrt{\alpha_0}+\sqrt{h_v(\gamma+\mu)})^2 \Leftrightarrow \sqrt{\beta_0}-\sqrt{\alpha_0} > \sqrt{h_v(\gamma+\mu)}.$$

This implies that $R_c > 1$ if and only if $R_g^n > 1$ when $\beta_0 > \alpha_0$.

References

[1] A.M. Stern, H. Markel, The history of vaccines and immunization: familiar patterns, new challenges, Health Aff. 24 (3) (2005) 611–621.
[2] P. Bonanni, Demographic impact of vaccination: a review, Vaccine 17 (1999) S120–S125.
[3] C.T. Bauch, Imitation dynamics predict vaccinating behaviour, Proc. R. Soc. B Biol. Sci. 272 (1573) (2005) 1669–1675.
[4] V.A.A. Jansen, N. Stollenwerk, H.J. Jensen, M.E. Ramsay, W.J. Edmunds, C.J. Rhodes, Measles outbreaks in a population with declining vaccine uptake, Science 301 (5634) (2003) 804.
[5] S. Gandon, T. Day, C.J.E. Metcalf, B.T. Grenfell, Forecasting epidemiological and evolutionary dynamics of infectious diseases, Trends Ecol. Evol. 31 (10) (2016) 776–788.
[6] K.D. McCormick, J.L. Jacobs, J.W. Mellors, The emerging plasticity of SARS-CoV-2, Science 371 (6536) (2021) 1306–1308.
[7] B. Bakhshandeh, Z. Jahanafrooz, A. Abbasi, M.B. Goli, M. Sadeghi, M.S. Mottaqi, M. Zamani, Mutations in SARS-CoV-2; consequences in structure, function, and pathogenicity of the virus, Microb. Pathog. 154 (2021) 104831.
[8] P.V. Markov, A. Katzourakis, N.I. Stilianakis, Antigenic evolution will lead to new SARS-CoV-2 variants with unpredictable severity, Nat. Rev. Microbiol. 20 (5) (2022) 251–252.
[9] T. Day, D.A. Kennedy, A.F. Read, S. Gandon, Pathogen evolution during vaccination campaigns, PLoS Biol. 20 (9) (2022) e3001804.
[10] S. Gandon, T. Day, The evolutionary epidemiology of vaccination, J. R. Soc. Interface 4 (16) (2007) 803–817.
[11] Q. Liu, Y. Xiao, A coupled evolutionary model of the viral virulence in an SIS community, Discrete Contin. Dyn. Syst.-B 28 (9) (2023) 5012–5036.
[12] Q. Liu, Y. Xiao, S.R. Smith?, The implications of host–pathogen co-evolutionary outcomes on macro-epidemics based on a combined-host strategy, Bull. Math. Biol. 87 (10) (2025) 1–28.
[13] S. Gandon, M.J. Mackinnon, S. Nee, A.F. Read, Imperfect vaccines and the evolution of pathogen virulence, Nature 414 (6865) (2001) 751–756.
[14] A. Walter, S. Gandon, S. Lion, Effect of unequal vaccination coverage and migration on long-term pathogen evolution in a metapopulation, J. Evol. Biol. 37 (2) (2024) 189–200.
[15] C. Ma, Y. Yang, J. Zu, Predicting the evolutionary and epidemiological dynamics of SARS-CoV-2 in South Africa, Virulence 16 (1) (2025) 2520335.
[16] Y. Yang, C. Ma, J. Zu, Coevolutionary dynamics of host-pathogen interaction with density-dependent mortality, J. Math. Biol. 85 (2) (2022) 15.
[17] T. Day, T. Parsons, A. Lambert, S. Gandon, The Price equation and evolutionary epidemiology, Philos. Trans. R. Soc. B 375 (1797) (2020) 20190357.
[18] T. Day, S. Gandon, Insights from Price's equation into evolutionary epidemiology, Dis. Evol. Models Concepts Data Anal. 71 (2006) 23–44.
[19] T. Day, S. Gandon, Applying population-genetic models in theoretical evolutionary epidemiology, Ecol. Lett. 10 (10) (2007) 876–888.
[20] C.T. Bauch, A.P. Galvani, D.J.D. Earn, Group interest versus self-interest in smallpox vaccination policy, Proc. Natl. Acad. Sci. 100 (18) (2003) 10564–10567.
[21] C.T. Bauch, D.J.D. Earn, Vaccination and the theory of games, Proc. Natl. Acad. Sci. 101 (36) (2004) 13391–13394.
[22] Y. Iwamura, J. Tanimoto, Realistic decision-making processes in a vaccination game, Phys. A Stat. Mech. Appl. 494 (2018) 236–241.
[23] M.R. Arefin, T. Masaki, K.M. Kabir, J. Tanimoto, Interplay between cost and effectiveness in influenza vaccine uptake: a vaccination game approach, Proc. R. Soc. A Math. Phys. Eng. Sci. 475 (2232) (2019).
[24] B. Wu, F. Fu, L. Wang, Imperfect vaccine aggravates the long-standing dilemma of voluntary vaccination, PloS One 6 (6) (2011) e20577.
[25] S.L. Chang, M. Piraveenan, M. Prokopenko, The effects of imitation dynamics on vaccination behaviours in SIR-network model, Int. J. Environ. Res. Public Health 16 (14) (2019) 2477.
[26] F. Fu, D.I. Rosenbloom, L. Wang, M.A. Nowak, Imitation dynamics of vaccination behaviour on social networks, Proc. R. Soc. B Biol. Sci. 278 (1702) (2011) 42–49.
[27] M.L. Ndeffo Mbah, J. Liu, C.T. Bauch, Y.I. Tekel, J. Medlock, L.A. Meyers, A.P. Galvani, The impact of imitation on vaccination behavior in social contact networks, PLoS Comput. Biol. 8 (4) (2012) e1002469.
[28] C. Gracia-Lázaro, A. Ferrer, G. Ruiz, A. Tarancón, J.A. Cuesta, A. Sánchez, Y. Moreno, Heterogeneous networks do not promote cooperation when humans play a Prisoner's Dilemma, Proc. Natl. Acad. Sci. 109 (32) (2012) 12922–12926.
[29] M.R. Arefin, T. Masaki, J. Tanimoto, Vaccinating behaviour guided by imitation and aspiration, Proc. R. Soc. A 476 (2239) (2020) 20200327.
[30] M.R. Arefin, J. Tanimoto, Imitation and aspiration dynamics bring different evolutionary outcomes in feedback-evolving games, Proc. R. Soc. A 477 (2251) (2021) 20210240.
[31] J. Du, B. Wu, L. Wang, Aspiration dynamics and the sustainability of resources in the public goods dilemma, Phys. Lett. A 380 (16) (2016) 1432–1436.
[32] T. Li, Y. Xiao, J. Heffernan, Linking spontaneous behavioral changes to disease transmission dynamics: behavior change includes periodic oscillation, Bull. Math. Biol. 86 (6) (2024) 73.
[33] M.A. Amaral, M.A. Javarone, Heterogeneous update mechanisms in evolutionary games: mixing innovative and imitative dynamics, Phys. Rev. E 97 (4) (2018) 042305.
[34] P. Poletti, M. Ajelli, S. Merler, Risk perception and effectiveness of uncoordinated behavioral responses in an emerging epidemic, Math. Biosci. 238 (2) (2012) 80–89.
[35] J.M. Heffernan, R.J. Smith, L.M. Wahl, Perspectives on the basic reproductive ratio, J. R. Soc. Interface 2 (4) (2005) 281–293.
[36] M.W. Hirsch, H.L. Smith, X.-Q. Zhao, Chain transitivity, attractivity, and strong repellors for semidynamical systems, J. Dyn. Differ. Equ. 13 (1) (2001) 107–131.
[37] S. Alizon, A. Hurford, N. Mideo, M. Van Baalen, Virulence evolution and the trade-off hypothesis: history, current state of affairs and the future, J. Evol. Biol. 22 (2) (2009) 245–259.
[38] A. Mougi, Y. Iwasa, Evolution towards oscillation or stability in a predator–prey system, Proc. R. Soc. B Biol. Sci. 277 (1697) (2010) 3163–3171.

[39] S. Marino, I.B. Hogue, C.J. Ray, D.E. Kirschner, A methodology for performing global uncertainty and sensitivity analysis in systems biology, J. Theor. Biol. 254 (1) (2008) 178–196.
[40] A. Mougi, Y. Iwasa, Unique coevolutionary dynamics in a predator–prey system, J. Theor. Biol. 277 (1) (2011) 83–89.
[41] J. Tanimoto, Sociophysics Approach to Epidemics, vol. 23, Springer, 2021.
[42] M. Mamun-Ur-Rashid Khan, J. Tanimoto, A new concept of optimal control for epidemic spreading by vaccination: technique for assessing social optimum employing Pontryagin's maximum principle, AIP Adv. 15 (7) (2025).
[43] C. Fraser, T.D. Hollingsworth, R. Chapman, F. de Wolf, W.P. Hanage, Variation in HIV-1 set-point viral load: epidemiological analysis and an evolutionary hypothesis, Proc. Natl. Acad. Sci. 104 (44) (2007) 17441–17446.
[44] C.-K. Li, H. Schneider, Applications of Perron–Frobenius theory to population dynamics, J. Math. Biol. 44 (5) (2002) 450–462.